N73-18003
NASA CR-2168

NASA CONTRACTOR REPORT

NASA CR-2168

DEVELOPMENT AND APPLICATIONS OF SUPERSONIC UNSTEADY CONSISTENT AERODYNAMICS FOR INTERFERING PARALLEL WINGS

by Kari Appa and G. C. C. Smith

Prepared by
BELL AEROSPACE COMPANY
Buffalo, N.Y. 14240
for Langley Research Center

NATIONAL AERONAUTICS AND SPACE ADMINISTRATION • WASHINGTON, D. C. • MARCH 1973

1. Report No.	2. Government Accession No.	3. Recipient's Catalog No.
NASA CR-2168		

4. Title and Subtitle	5. Report Date
DEVELOPMENT AND APPLICATIONS OF SUPERSONIC UNSTEADY CONSISTENT AERODYNAMICS FOR INTERFERING PARALLEL WINGS	March 1973
	6. Performing Organization Code
7. Author(s)	8. Performing Organization Report No.
Kari Appa and G. C. C. Smith	
9. Performing Organization Name and Address	10. Work Unit No.
Bell Aerospace Company Buffalo, New York 14240	501-22-04-01
	11. Contract or Grant No.
	NAS1-10880
12. Sponsoring Agency Name and Address	13. Type of Report and Period Covered
National Aeronautics and Space Administration Washington, D. C. 20546	Contractor Report
	14. Sponsoring Agency Code

15. Supplementary Notes

16. Abstract

The analytical development of unsteady supersonic aerodynamic influence coefficients for isolated and nearly parallel interfering coplanar and noncoplanar wings is described. Numerical formulations based on triangular discretizations of wings and diaphragms are handled in a kinematically consistent manner. Examples of isolated wing cases are compared with respect to aerodynamic influence coefficients and flutter boundaries. Aerodynamic influence coefficients for interfering wings are compared where corresponding results are available.

Computer programs for the interfering case are described in a companion User's Manual, Bell Aerospace Report No. 2471-956003, and presented in a Programmer's Manual, Bell Aerospace Report No. 2471-956004.

17. Key Words (Suggested by Author(s))	18. Distribution Statement
Flutter, Supersonic Finite element unsteady aerodynamics Interfering wings	Unclassified - Unlimited

19. Security Classif. (of this report)	20. Security Classif. (of this page)	21. No. of Pages	22. Price*
Unclassified	Unclassified	56	$ 3.00

*For sale by the National Technical Information Service, Springfield, Virginia 22151

FOREWORD

This report describes developments in the analytical determination of unsteady supersonic aerodynamics for a class of interfering wings using a triangular element representation of wings and diaphragms.

The work was accomplished by Bell Aerospace Company under Contract NAS 1-10880 with the National Aeronautics & Space Administration, Langley Research Center, Hampton, Virginia. G.C.C. Smith was Program Manager and Dr. Kari Appa was the Principal Investigator. A. A. Paine wrote the associated computer programs (Ref 28).

The following program documents are relevant to this report:

USER'S MANUAL - NASA CR-112184

PROGRAMMER'S MANUAL - NASA CR-112185

The authors acknowledge permission from the Air Force to publish data from References 11 and 19.

CONTENTS

ILLUSTRATIONS

TABLES

DEVELOPMENT AND APPLICATIONS OF SUPERSONIC UNSTEADY CONSISTENT AERODYNAMICS FOR INTERFERING PARALLEL WINGS

by

Kari Appa * and G. C. C. Smith +

Bell Aerospace Company

Division of Textron Inc.

SUMMARY

The analytical development of unsteady supersonic aerodynamic influence coefficients, (AIC's), for isolated and nearly parallel interfering coplanar and noncoplanar wings is described. Numerical formulations based on triangular discretizations of wings and diaphragms are handled in a kinematically consistent manner. Examples of isolated wing cases are compared with respect to AIC's and flutter boundaries. AIC's for interfering wings are compared where corresponding results are available.

Computer programs for the interfering case are described in a companion User's Manual, NASA CR-112184, and presented in a Programmer's Manual, NASA CR-112185.

INTRODUCTION

The evaluation of aeroelastic effects requires accurate determination of oscillatory aerodynamic, stiffness and inertia properties of a flight vehicle. Stiffness and inertia properties of geometrically complex structures may be computed to a high degree of accuracy using modern finite element methods. The determination of unsteady aerodynamic forces in various flow regimes on the other hand, involves more complex differential equations, and their integral solution equivalents. Satisfactory solutions, analytical for simple planforms, and numerical for more complex planforms have evolved for isolated planar wings. Much effort has been devoted to more complex situations involving intersecting surfaces, interfering surfaces, dihedralled surfaces, and wing-body interference. The summary papers of References 1 and 2 attest to the intensive interest and efforts applied.

Garrick and Rubinow (Ref 3) pioneered the development of solutions to such boundary value problems by the superposition of elementary solutions of the nature of pulsating acoustic sources distributed on the boundaries, from which have developed many techniques discussed in the literature. References 1 and 2 indicate that integration of the differential/integral equations for practical and increasingly complicated wing and wing-body configurations is a significant problem even with present day computational facilities. Therefore, numerical integration methods are continually being modified and improved.

---

* Chief, Dynamic Analysis

+ Chief Engineer, Structural Dynamics

In supersonic flow, numerical integration procedures have been based on the representation of domains of dependence in terms of discrete "elements" of various types in each of which the downwash has generally been approximated as a constant.

These types include

- square boxes (e.g., Pines, Dugundji and Neuringer, (Ref 4)) in which the sides are parallel and normal to the free stream

- characteristic boxes (e.g., Smith (Ref 5) and Zartarian, Hsu and Voss (Ref 6)) in which parallelogram elements have their sides parallel to the Mach lines

- rectangular ("Mach") boxes (e.g., Li, Ref 7) such that the box diagonals are parallel to the Mach lines.

Zartarian and Hsu (Ref 8) made extensive studies on the application of rectangular, characteristic and Mach box methods, and discussed various working rules for the application of the Mach box method.

Ashley (Ref 9) described the application of superposition methods to interfering surfaces and the use of Mach box methods for intersecting planes.

Moore and Andrew (Ref 10) and Donato and Huhn (Ref 11) developed computer programs to calculate the velocity potentials and generalized forces for isolated, interfering and intersecting planes. Stark (Ref 12) contributed very significantly to the evaluation of downwash terms along a subsonic leading edge in the characteristic box approach.

The general approaches listed above have at least two obvious factors leading to inaccuracies in numerical computations

- the planform and associated diaphragm boundaries cannot be well represented with elements tied to characteristic or flow directions

- the approximation of constant downwash within an element.

While both inaccuracies can be alleviated by the use of a larger number of smaller elements, it is obvious that this is at the expense of a large increase in the number of equations to be handled, and will result in rapidly increasing computational effort.

Appa and Smith in References 13 and 14 have discussed a different approach to planform and diaphragm discretization and numerical procedures which have the following advantages over the methods referred to above:

- constancy of the wing grid system at all Mach numbers

- continuous distribution of downwash terms across element boundaries

- well-represented wing and diaphragm boundaries

- flexibility in the choice of diaphragm elements

- consistent aerodynamic forces via the principle of virtual work

- convenient aeroelastic formulation for flutter synthesis problems (e.g., optimization)

The following sections relate to analytical developments and computer applications for such a method in the case of isolated and interfering nearly parallel coplanar and noncoplanar wings at supersonic Mach numbers.

Results for unsteady aerodynamic forces from the present method are compared with published data from other methods.

Additionally, the method is applied to flutter of planar isolated and interfering wings and compared (for isolated wings) to experimental results.

The general intent of the work is to illustrate the potential for more economic and accurate determination of supersonic unsteady aerodynamics particularly for complex configurations.

An operational computer program which was developed in the course of the work has been used on IBM 360/65 and CDC6600.

SYMBOLS

$\mathbf{A}', \mathbf{B}', \mathbf{A}, \mathbf{B}$	Element and system pressure matrices
a	A Boolean matrix describing topological connections of the elements in the structure
a_o	Speed of sound in free stream
a_u, a_ℓ	Slopes of the upper and lower sides of a triangle
b_u, b_ℓ	Constants in the equations for upper and lower sides of a triangle
b_o	Semichord (as in Ref. 21)
c	Wing chord, Figures 3, 4, 5
F	Kernel, defined by equation (5)
I	Integrals; also unit matrix
$k = \frac{\omega \ell}{U}$	Reduced frequency
$\hat{k}$	$= \frac{kM^2}{\beta^2}$
K	Stiffness matrix
ℓ	Reference length
M	Mass matrix
M_o	Mach number
$\vec{n}$	Unit normal vector
n	Number of degrees of freedom
N	Number of terms in interpolation or modal series
$\bar{N}$	Summation variable
p	Pressure
p	Nodal force vector

SYMBOLS (CONT)

q	Displacement vector
q_o	Dynamic pressure, q_o^* a reference pressure = $\frac{1}{2} \rho_o^* a_o^{*2} M_o^2$
$Q, \tilde{Q}$	Generalized aerodynamic coefficients, discrete and interpolated, respectively
S	Surface of integration
r, s	Hyperbolic radii, Eqn (6)
t	Dimensional time
T	Transformation matrix
U	Flight speed
w	Downwash velocity
W	Induced downwash influence coefficient matrix
$\tilde{W}$	Virtual work
x, y, z	Dimensionless rectangular coordinates
$\bar{x}, \bar{z}$	x and z coordinates of apex of tailplane (see Fig. 9)
$X = (x, y, z)$	Position vector of receiving point
$\bar{Z}(x, y, t)$	Displacement in space-time, nondimensional, referred to ℓ
$Z(x, y)$	Displacement amplitude (nondimensional)
α	Damping rate; (see λ)
β	$= (M_o^2 - 1)^{\frac{1}{2}}$
$\Gamma, \tilde{\Gamma}$	Transformation Matrices Eqns (19), (38)
δ	$= q_o^*/q_o$, dynamic pressure ratio
$\bar{\eta}$	A column vector of generalized coordinates
λ	$= \alpha + i\omega$
$\bar{\lambda}$	$\frac{\lambda \ell}{U} = \frac{\alpha \ell}{U} + i\frac{\omega \ell}{U}$, a complex reduced frequency

μ	Ratio of structural mass to air mass
μ, ν	Defined by Eqn. (A7)
ξ, η, ζ	Dimensionless running coordinates in the fore Mach cone
$\Xi = (\xi, \eta, \zeta)$	Position vector of source in the fore Mach cone
ρ	Density of air
$\boldsymbol{\rho}$	Kinematic displacement vector of an element
σ	Source strength (scalar)
$\boldsymbol{\sigma}$	A column vector of source strength at nodes of elements, and the complete system
φ	Velocity Potential - a scalar
$\boldsymbol{\phi}$	Column Vector of Velocity potential
$\boldsymbol{\Phi}$	Element V.I.C. Matrix relating velocity potential to displacement for isolated wings, and to source strength for interfering wings (see Eqns. 11 and A-5 respectively)
χ	Transformation Matrix of Natural Modes
ψ	Defined in Eqn. (A-9)
$\boldsymbol{\Psi}$	System source strength to system displacement transformation matrix
ω	Circular frequency, radians per second
$\tilde{\omega}$	$\frac{2}{7}\frac{\omega a_o}{U}$ as defined in Ref. 22
Ω	An interpolation matrix
Subscripts	
cr	Critical
i, j	Denote elements or summation variables
ℓ, m	Denote modal numbers
n, r	Summation variables
Re, Im	Real and imaginary parts

R	Reference value
s	Wake
ℓ, u	Lower and upper limits
η	Derivative with respect to η

Superscripts

d	Diaphragm
L, U	Lower, Upper
t	Transpose
w	Wing
*	Sea level value (indent on ρ, q_o, a_o)

Notation

$\left\| \quad \right\|$	A column vector
[ ]	A matrix
$\lceil \quad \rfloor$	A diagonal matrix
$[\ ]^t$	Transpose of a matrix
$[\ ]^{-1}$	Inverse of a matrix
Δ ( )	Difference between upper and lower value

Note: In general terms, a lower case symbol represents a continuous variable, a bold-faced symbol with subscript/superscript represents an element nodal value matrix, a bold-faced symbol without subscript represents a "system" matrix (i.e., that resulting from assembly of all element nodal matrices). This usage applies to p, q, w, ρ, σ, φ, ψ, in particular.

DEVELOPMENT OF THE METHOD

Detailed derivation and some applications of "finite element" idealizations to the determination of unsteady aerodynamic coefficients appear in References 13 and 14. Application to isolated and interfering planar wings is given in this report. The basic elements used to represent the planform of a wing in a discretized form may be quadrilateral and triangular elements. However, the simpler triangular element forms the basis in this work. The elements can be of different sizes and orientations to "best fit" both wings (independent of Mach number) and diaphragms.

In finite element analysis, functionals within an element are expressed in terms of nodal (discrete) values and derivatives at the nodes by means of interpolation functions. The accuracy of the analysis depends on the degree to which the properties of continuity of the functionals across the element boundaries are satisfied. This is related to the order of appearance of the functional and its derivatives in the integral equation. Since no derivatives of source functionals are involved in the determination of potential, source strength distribution is taken to be expressed linearly within the elements in terms of their nodal values.

Since modal data are also frequently expressed as discrete nodal displacements, the virtual work integrals determined in this work use linearly interpolated potential and modal data to give linearly consistent generalized forces.

Velocity Potential

The linearized equations of motion in unsteady supersonic flow referenced to a rectangular coordinate system, Figure 1, are given by

$$(1-M_o^2)\frac{\partial^2\varphi}{\partial x^2}+\frac{\partial^2\varphi}{\partial y^2}+\frac{\partial^2\varphi}{\partial z^2}=\frac{2M_o}{a_o}\frac{\partial^2\varphi}{\partial x\partial t}+\frac{1}{a_o^2}\frac{\partial^2\varphi}{\partial t^2} \tag{1}$$

where φ, M_o and a_o represent the perturbation velocity potential, Mach number and speed of sound respectively. Solutions to equation (1) are sought for harmonic motion of the lifting surface. In many common flutter solution procedures the eigenvalue solutions subsequently determined using assumed real reduced frequency aerodynamics are complex (implying diverging and decaying oscillations) for which the aerodynamics are inconsistent. This suggests, (compare Richardson, Reference 15) the formal determination of aerodynamics for complex exponential motions, which, though not carried through to flutter solutions herein, requires motion of the lifting surface in the form

$$\bar{Z}(x, y, t) = Z(x, y)\, e^{\lambda t} \tag{2}$$

where $\lambda = (\alpha + i\omega)$, (3)

and α is a damping factor, and ω the circular frequency of oscillation. (See also Ref. 16).

The deflection $\bar{Z}$ is related to the source strength through boundary conditions discussed later (see for example, Eqn. 13).

The solution for the velocity potential following Reference 3 is given by

$$\varphi(X,t) = -\frac{U\ell}{\pi}\iint_S F(X,\Xi)\,\sigma(\Xi)\,d\xi\,d\eta\,e^{\lambda t} \tag{4}$$

where $F(X,\Xi) = \dfrac{\exp\left(\dfrac{-\ell\lambda M_0^2}{U\beta^2}(x-\xi)\right)\cdot\cosh\left(\dfrac{\ell\lambda M_0}{U\beta^2}(r\cdot s)^{1/2}\right)}{(r\cdot s)^{1/2}}$ (5)

is the kernel function,

$$\left.\begin{aligned} r &= (x-\xi)-\beta\left[(y-\eta)^2+(z-\zeta)^2\right]^{1/2} \\ s &= (x-\xi)+\beta\left[(y-\eta)^2+(z-\zeta)^2\right]^{1/2} \end{aligned}\right\} \tag{6}$$

are hyperbolic radii and $\sigma(\Xi)$ is the nondimensional source strength distribution. The symbols $X = (x, y, z)$ and $\Xi = (\xi, \eta, \zeta)$ denote respectively the vector positions (dimensionless with respect to ℓ) at which the velocity potential is evaluated and the influence source strength is situated. The surface integration in equation (4) covers the lifting surface and associated diaphragm regions in the fore Mach cone emerging from X. Generally, closed form integration of (4) is not possible, and numerical integration techniques using various "box" schemes are employed. In the current analysis, the integration area is divided into a number of triangular elements (Figure 1). Summing over all elements the velocity potential within an element i may be written

$$\varphi(X_i,t) = -\frac{U\ell}{\pi}\sum_j \iint_{S_j} F(X_i\,\Xi_j)\cdot\sigma(\Xi_j)\cdot d\xi\,d\eta\cdot e^{\lambda t} \tag{7}$$

where the subscripts i and j denote receiving element i and influencing element j respectively. By means of interpolation functions $\Omega(\Xi)$ the source strength distribution $\sigma(\Xi_j)$ within an influencing element can be expressed as a linear combination of its nodal values σ_j as

$$\sigma(\Xi_j) = \Omega(\Xi)\,\sigma_j \tag{8}$$

where Ω, (see Eqn. A-2) is a row matrix of interpolation functions and σ_j is a column vector of nodal values. The nodal values of the source strength for each element can be abstracted from a system source vector σ by

$$\sigma_j = a_j\,\sigma \tag{9}$$

in which a_j is a Boolean Matrix (Ref 17) related to the topological assembly of the elements. Summing over all the elements in the fore Mach cone region, the velocity potentials at the nodes of the receiving elements are given by

$$\phi_i = -U\ell\sum_j \Phi_{ij}\,a_j\,\sigma \tag{10}$$

where σ is a nondimensional nodal source vector and

$$\Phi_{ij} = \frac{1}{\pi}\iint_{S_j} F(X_i,\Xi_j)\;\Omega(\Xi)\,dS \tag{11}$$

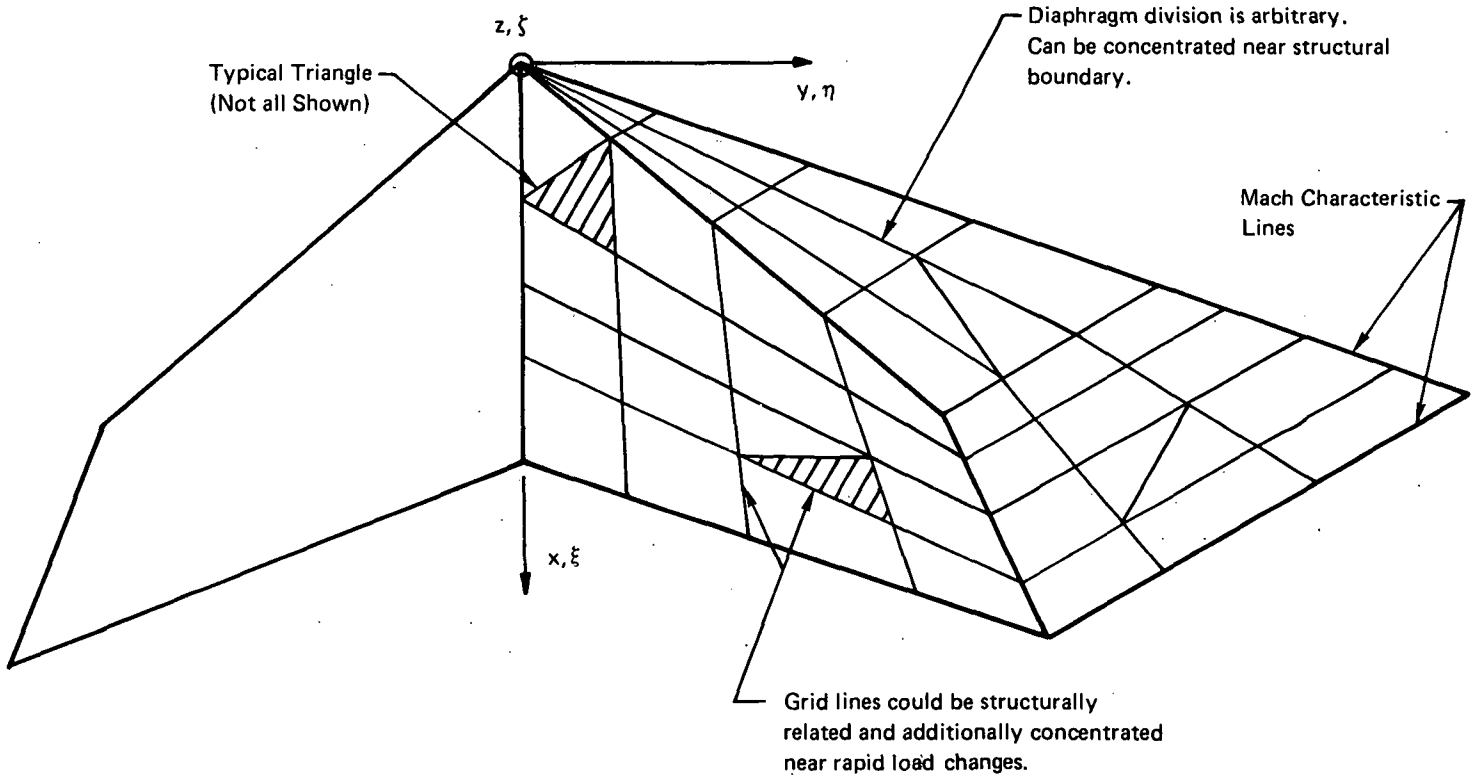

Figure 1. Layout of Grid System

is the velocity potential influence coefficient matrix for the ith element nodes due to the source distribution in the jth element. Numerical integration of Φ_{ij} is described in the Appendix. Then considering all the elements, the velocity potential for the system can be written as

$$\phi = -U\ell\,[\Phi]\,\{\sigma\} \tag{12}$$

where ϕ is a column vector of nodal velocity potentials and Φ is the total velocity potential influence coefficient matrix.

Boundary Conditions

The source strength nodal vector σ in Eq. (12) must be such that the following boundary conditions are satisfied:

- the kinematic boundary condition on the lifting surface given by

$$\frac{\partial \varphi}{\partial \vec{n}}\, e^{\lambda t} = \ell \frac{D\bar{Z}}{Dt} \tag{13}$$

where

$\frac{\partial \varphi}{\partial \vec{n}}$ is the derivative of the velocity potential normal to the surface at the field point X,

and

$$\frac{D}{Dt} = \frac{\partial}{\partial t} + \frac{U}{\ell}\frac{\partial}{\partial x} \tag{14}$$

is the material derivative in the streamwise direction.

- in the case of a subsonic leading edge, the velocity potential difference in the diaphragm

$$\Delta\phi_d = (\phi_{upper} - \phi_{lower})_d \text{ must be zero} \tag{15}$$

- the pressure difference in the wake

$$\Delta p_s = (p_{upper} - p_{lower})_s \text{ must be zero.} \tag{16}$$

The boundary conditions for interfering wings require special considerations described later.

Subsonic Leading Edge Case

Antisymmetry of the nodal source distribution σ and of ϕ with respect to the plane of the wing in the lifting case implies that Equations (12) and (13) may be used to relate potential and source strength jumps in partitioned matrix notation as

$$\begin{Bmatrix} \Delta\phi_w \\ \Delta\phi_d \end{Bmatrix} = -U\ell \begin{bmatrix} \Phi_{ww} & \Phi_{wd} \\ \Phi_{dw} & \Phi_{dd} \end{bmatrix} \begin{Bmatrix} \Delta\sigma_w \\ \Delta\sigma_d \end{Bmatrix} \tag{17}$$

where the subscripts 'w' and 'd' denote the nodes situated on the wing and diaphragm respectively. Since in the diaphragm $\Delta\phi_d = 0$ (Ref. 18), the source strength vector $\Delta\sigma_d$ from the second of Equation (17) is

$$\left\{\Delta\sigma_d\right\} = -\Gamma\left\{\Delta\sigma_w\right\} \tag{18}$$

where

$$\Gamma = \Phi_{dd}^{-1}\,\Phi_{dw} \tag{19}$$

Using this solution in the first set of matrix Equation (17), the velocity potential distribution on the lifting surface is given by

$$\Delta\phi_w = -U\ell\,\widetilde{\Phi}_{ww}\,\Delta\sigma_w \tag{20}$$

in which

$$\widetilde{\Phi}_{ww} = \Phi_{ww} - \Phi_{wd}\,\Gamma \tag{21}$$

Kinematic Boundary Conditions

The Isolated Wing Case

It is shown in Ref. 3 that the source strength distribution, $\sigma\, e^{\lambda t}$ is proportional to the downwash $\ell\frac{D\bar{Z}}{Dt} = w e^{\lambda t}$. Let ρ_j denote a column vector of nodal kinematic deformation modes of an element j in the fore Mach cone region. Then the interpolated deformation within the element j can be expressed in terms of the element nodal values as

$$\bar{Z}(\xi_j, \eta_j, t) = \Omega(\xi, \eta)\rho_j\, e^{\lambda t} \tag{22}$$

If the mean position of the lifting surface is parallel to the x-y plane, the downwash from Eq. (13) is

$$\frac{1}{\ell}\frac{\partial\varphi}{\partial\zeta}\, e^{\lambda t} = w e^{\lambda t} = \ell\left(\frac{\partial}{\partial t} + \frac{U}{\ell}\frac{\partial}{\partial\xi}\right)\bar{Z} \tag{23}$$

or in nondimensional form using Equation (22)

$$\frac{w(\xi_j, \eta_j)}{U} = (\bar{\lambda}\Omega + \Omega_\xi)\rho_j \tag{24}$$

in which $\bar{\lambda} = \left(\frac{\alpha\ell}{U} + \frac{i\omega\ell}{U}\right)$ is the complex reduced frequency, and

$$\Omega_\xi = \frac{\partial\Omega}{\partial\xi}. \tag{25}$$

Thus for the isolated case, the source strength distribution $\sigma e^{\lambda t}$ in Equation (4) will be replaced by

$$\sigma(\Xi_j) = (\bar{\lambda}\,\Omega + \Omega_\xi)\,\rho_j \tag{26}$$

Utilizing the relation between element nodal displacements ρ_j and system displacements q as given by the Boolean matrix a_j

$$\rho_j = a_j q \tag{27}$$

the system velocity potential analogous to Eq. (12) may be expressed in matrix form as

$$\Delta\phi = -2U\ell\,[\Phi]\,q \tag{28}$$

Interfering Nearly Parallel Wings

The determination of source strengths in the case of interfering planes is more complex than in the isolated case. Ashley in Reference 9 has discussed in detail some practical assumptions for relating the source strength distribution to the kinematic boundary conditions. In the present analysis the following assumptions based on Reference 9 are made:

(i) convenient diaphragms can be established between the lifting surfaces and the Mach hyperbolae

(ii) induced normal wash at one diaphragm due to the presence of the second lifting surface can be disregarded.

Considering two planar interfering wings (Figure 2), the source distribution σ^{L}_{1w} on the lower surface of wing 1 and σ^{U}_{2w} on the upper surface of wing 2 are unaffected by the interference. Then these source strengths using Eq. 23 can be expressed as

$$\sigma^{L}_{1w} = -\frac{\ell}{U}\frac{D\bar{Z}_1}{Dt} \tag{29}$$

and

$$\sigma^{U}_{2w} = \frac{\ell}{U}\frac{D\bar{Z}_2}{Dt} \tag{30}$$

The source strength distributions on the upper surface of wing 1 and the lower surface of wing 2, because of interference, are modified by the induced downwash in their respective planes. The induced downwash on the upper surface of wing 1 due to source distributions on the lower surface of wing 2 and its diaphragm may be written as

$$w_{12} = W_{12w}\,\sigma^{L}_{2w} + W_{12d}\,\sigma^{L}_{2d} \tag{31}$$

where

w_{12} is a nodal column vector of induced downwash on wing 1 and its diaphragm

W_{12} is the velocity influence coefficient matrix for the wing 1 due to interference of source distributions on the lower surface of wing 2 and its diaphragm.

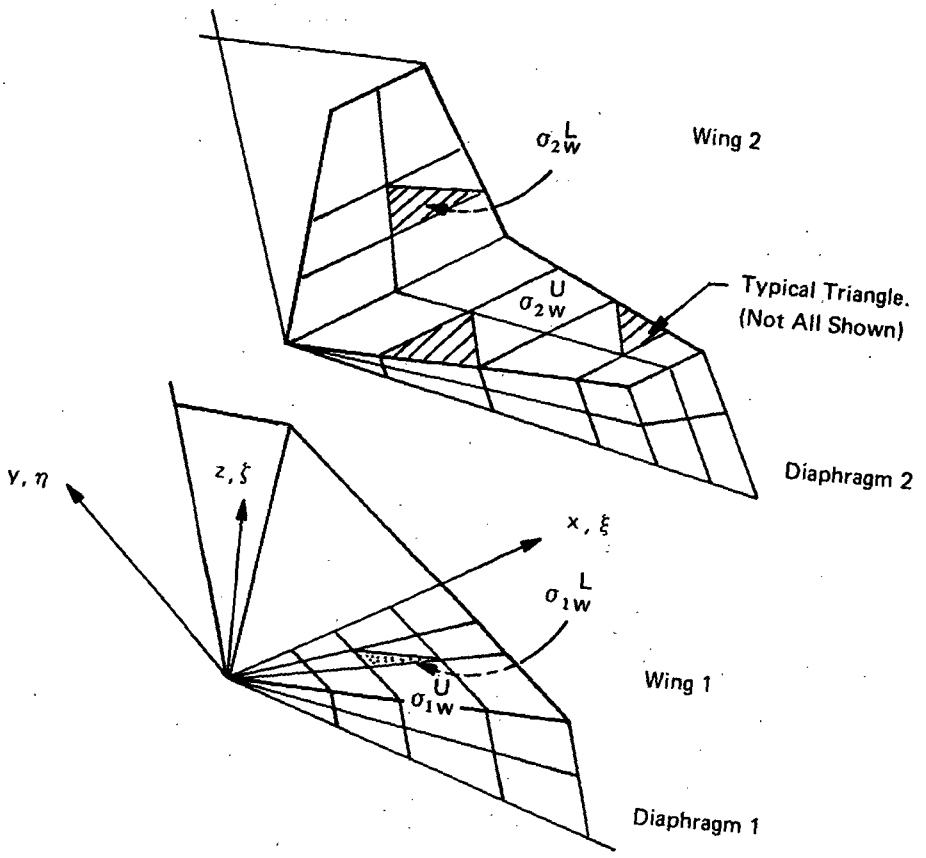

Figure 2. Layout of Grid System – 2 Wings

The subscripts w and d denote control points on the wing and its associated diaphragms, and the superscripts U and L denote upper and lower surfaces, respectively. Derivation and numerical integration of the downwash influence coefficient matrix W_{ij} for the triangular element is described in the Appendix (see Eqs. A13-A20).

In the following work, in accord with assumption (ii), the effect of induced downwash w_{12} in the diaphragm has been disregarded. Since the wing planes are assumed to be nearly parallel, the side wash contribution to the computation of w_{12} has also been neglected. Then the source strength required to satisfy the total normal velocity condition on the upper surface of wing 1 is given by

$$\sigma^{U}_{1w} = \frac{\ell}{U}\frac{D\tilde{Z}_1}{Dt} - W_{12w}\,\sigma^{L}_{2w} - W_{12d}\,\sigma^{L}_{2d} \tag{32}$$

Similarly the required source strength distribution on the lower surface of wing 2 is given by

$$\sigma^{L}_{2w} = -\left[\frac{\ell}{U}\frac{D\tilde{Z}_2}{Dt} - W_{21w}\,\sigma^{U}_{1w} - W_{21d}\,\sigma^{U}_{1d}\right] \tag{33}$$

Eqs. (32) and (33) can be rearranged as

$$\begin{bmatrix} I_{11} & W_{12w} \\ -W_{21w} & I_{22} \end{bmatrix} \begin{Bmatrix} \sigma^{U}_{1w} \\ \sigma^{L}_{2w} \end{Bmatrix} = \begin{Bmatrix} \frac{\ell}{U}\frac{D\tilde{Z}_1}{Dt} \\ \frac{-\ell}{U}\frac{D\tilde{Z}_2}{Dt} \end{Bmatrix} + \begin{bmatrix} 0 & -W_{12d} \\ W_{21d} & 0 \end{bmatrix} \begin{Bmatrix} \sigma^{U}_{1d} \\ \sigma^{L}_{2d} \end{Bmatrix} \tag{34}$$

The relation between the source strengths in the diaphragm and wing is given by Equation (18). Re-writing this equation as

$$\begin{Bmatrix} \sigma^{U}_{1d} - \sigma^{L}_{1d} \\ \sigma^{U}_{2d} - \sigma^{L}_{2d} \end{Bmatrix} = -\left[\Gamma\right] \begin{Bmatrix} \sigma^{U}_{1w} - \sigma^{L}_{1w} \\ \sigma^{U}_{2w} - \sigma^{L}_{2w} \end{Bmatrix} \tag{35}$$

and using the condition of downwash continuity in the diaphragm, i.e.,

$$\sigma^{U}_{d} = -\sigma^{L}_{d} \tag{36}$$

the required source strength in the diaphragm may be written as

$$\begin{Bmatrix} \sigma^{U}_{1d} \\ \sigma^{L}_{2d} \end{Bmatrix} = \left[\tilde{\Gamma}\right] \begin{Bmatrix} \sigma^{U}_{1w} \\ \sigma^{L}_{2w} \end{Bmatrix} - \left[\tilde{\Gamma}\right] \begin{Bmatrix} \sigma^{L}_{1w} \\ \sigma^{U}_{2w} \end{Bmatrix} \tag{37}$$

where

$$\tilde{\Gamma} = \frac{1}{2} \begin{bmatrix} -I & 0 \\ 0 & I \end{bmatrix} \begin{bmatrix} \Gamma \end{bmatrix} \begin{bmatrix} I & 0 \\ 0 & -I \end{bmatrix} \tag{38}$$

Eqs. (29) and (30) then give

$$\begin{Bmatrix} {}^{U}\sigma_{1d} \\ {}^{L}\sigma_{2d} \end{Bmatrix} = \begin{bmatrix} \tilde{\Gamma} \end{bmatrix} \begin{Bmatrix} {}^{U}\sigma_{1w} \\ {}^{L}\sigma_{2w} \end{Bmatrix} + \begin{bmatrix} \tilde{\Gamma} \end{bmatrix} \begin{Bmatrix} \frac{\ell}{U} \frac{D\tilde{Z}_1}{Dt} \\ \frac{\ell}{U} \frac{D\tilde{Z}_2}{Dt} \end{Bmatrix} \tag{39}$$

Substituting for ${}^{U}\sigma_{1d}$ and ${}^{L}\sigma_{2d}$ in Eq. (34), the following matrix equation is obtained:

$$\left[\begin{bmatrix} I_{11} & W_{12w} \\ -W_{21w} & I_{22} \end{bmatrix} - \begin{bmatrix} 0 & -W_{12d} \\ W_{21d} & 0 \end{bmatrix} \begin{bmatrix} \tilde{\Gamma} \end{bmatrix} \right] \begin{Bmatrix} {}^{U}\sigma_{1w} \\ {}^{L}\sigma_{2w} \end{Bmatrix} = \begin{Bmatrix} \frac{\ell}{U} \frac{D\tilde{Z}_1}{Dt} \\ \frac{-\ell}{U} \frac{D\tilde{Z}_2}{Dt} \end{Bmatrix} + \begin{bmatrix} 0 & -W_{12d} \\ W_{21d} & 0 \end{bmatrix} \begin{bmatrix} \tilde{\Gamma} \end{bmatrix} \begin{Bmatrix} \frac{\ell}{U} \frac{D\tilde{Z}_1}{Dt} \\ \frac{-\ell}{U} \frac{D\tilde{Z}_2}{Dt} \end{Bmatrix} \tag{40}$$

The input downwash terms $\frac{\ell}{U} \frac{D\tilde{Z}_i}{Dt}$ are calculated for the system structural displacements q at each grid point, and the slopes $\frac{\partial q}{\partial x}$, by

$$\frac{\ell}{U} \frac{D\tilde{Z}_i}{Dt} = \lambda \{ q \} + \left\{ \frac{\partial q}{\partial x} \right\} \tag{41}$$

Using Eq. (41) in Eqs. (29), (30) and (40), the difference in the source distribution across the wing surfaces can be written as

$$\{ \Delta \sigma_w \} = [\Psi] \{ q \} \tag{42}$$

where Ψ is a transformation matrix relating source strength and displacement vectors. The velocity potential differences across the wing surfaces are then obtained by substitution of Eq. (42) into Eq. (20).

Concerning Subsonic Trailing Edges

In this case the source strength distribution in the wake can be determined from the pressure continuity condition across the wake sheet and the trailing edge potentials. It may then be expressed in terms of the distribution on the wing and diaphragm and condensation of velocity potential in the wake performed similar to Equation (21).

For interfering cases, induced downwash matrices can similarly be modified. However, the subsonic trailing edge case has not been included in the present analyses and programs.

Consistent Nodal Forces

The velocity potential within the i^{th} element can be expressed in terms of nodal values $\Delta\phi_i$ and the interpolation matrix Ω as

$$\Delta\varphi(X_i) = [\,\Omega\,]\,\{\,\Delta\phi_i\,\}\,e^{\lambda t} \tag{43}$$

Since the pressure distribution within the i^{th} element from the linearized Bernoulli's equation is given by

$$p(X_i)\,e^{\lambda t} = \rho\left[\frac{\partial}{\partial t} + \frac{U}{\ell}\,\frac{\partial}{\partial x}\right]\,\Delta\varphi(X_i) \tag{44}$$

from Equations (43), (23), (24), the pressure distribution is

$$p(X_i) = +\frac{\rho U}{\ell}\,[\,\bar{\lambda}\,\Omega + \Omega_x\,]\,\Delta\phi_i \tag{45}$$

The virtual work done on the i^{th} element by the pressure through virtual displacement $\ell\delta Z(X_j)$ using Eq. (22) is

$$\delta\tilde{W}_{ji} = \rho U\ell^2 \cdot \delta\rho_j{}^t \iint_{S_i}[\bar{\lambda}\,\Omega^t\,\Omega + \Omega^t\,\Omega_x]\;dx\,dy\;\Delta\phi_i \tag{46}$$

Summing over all elements on the lifting surface and using Eq. (28), the virtual work principle yields the nodal forces,

$$\begin{aligned} p &= \rho\,U\ell\,[\,\bar{\lambda}\,A + B\,]\,\Delta\phi \\ &= -2\rho U^2\ell^2\,[\,\bar{\lambda}\,A + B\,]\,[\,\Phi\,]\,q \end{aligned} \tag{47}$$

where A and B, real pressure matrices, are assemblies of element matrices defined by

$$A = \sum_n a_n^t\,A_n\,a_n \tag{48}$$

$$B = \sum_n a_n^t\,B_n\,a_n \tag{49}$$

The element matrices are given by

$$A_j = \iint_{S_j}\Omega^t\,\Omega\,dS \tag{50}$$

$$B_j = \iint_{S_j} \Omega^t \Omega_x \, dS \tag{51}$$

and 'n' represents summation over wing elements only.

Generalized Forces

If q_ℓ and q_m denote two nondimensional nodal deformation modes, the virtual work done in a virtual displacement δq_ℓ is, using Eq. (47)

$$\begin{aligned} \delta \tilde{W}_{\ell m} &= \ell \delta q_\ell^{\,t} \, p_m \\ &= -2\rho \, U^2 \, \ell^3 \, \delta q_\ell^{\,t} \, [\, \bar{\lambda} \, A + B \,] \, [\, \Phi \,] \, q_m \\ &= -2\rho \, U^2 \, \ell^3 \, \delta q_\ell^{\,t} \, \tilde{Q}_{\ell m} \, q_m \qquad \text{say.} \end{aligned} \tag{52}$$

The matrix of dimensionless generalized force coefficients is then defined by

$$-\frac{1}{2\rho \, U^2 \, \ell^3} \frac{\partial}{\partial q_\ell} \left(\frac{\partial \tilde{W}_{lm}}{\partial q_m} \right) = \tilde{Q}_{\ell m}, \tag{53}$$

the elements of $\tilde{Q}$.

FLUTTER ANALYSIS

The flutter equations of motion for a flight structure may be written

$$\mathbf{Kq} + \mathbf{M\ddot{q}} + 4\, q_o \ell\, A(k,M_o)\mathbf{q} = 0 \tag{54}$$

where K, M, A are (nxn) stiffness, inertia and aerodynamic matrices respectively,

$\mathbf{q}$ is a (nxl) displacement vector

ℓ is a reference length

$q_o = \frac{\rho U^2}{2} = \frac{\rho a_o^2 M_o^2}{2}$ is the dynamic pressure and

$k = \frac{\omega \ell}{U}$ is the reduced frequency

ρ is the air density

U is the true flight speed.

For small oscillations, the deformation of the structure can be approximated by a linear combination of a few of the lower frequency natural modes as

$$\mathbf{q} = \chi \bar{\eta} \tag{55}$$

where χ is a nxN modal matrix, (N<<n) and $\bar{\eta}$ is a vector of generalized coordinates. Taking the motion to be of the form

$$\bar{\eta} = \eta e^{\lambda t} \tag{56}$$

Eqn (54) becomes, for zero damping at the flutter boundary ($\alpha = 0$),

$$K_{ii}\eta_i - \omega^2 M_{ii}\eta_i + 4q_o \ell \sum_j Q_{ij}(k, M_o)\eta_j = 0 \tag{57}$$

for i = 1 . . . N, where K_{ii}, M_{ii} and Q_{ij} are the generalized stiffness, inertia and aerodynamic matrix coefficients respectively.

Using a reference frequency ω_R and a reference dynamic pressure $q_o^* = \frac{\rho_o^* a_o^{*2} M_o^2}{2}$,

where * parameters refer to sea level condition, say, Eqn (57) can be rewritten in nondimensional form as

$$\left[\left[\left(\frac{\omega_i}{\omega_R} \right)^2 \right] + \delta \left(\frac{4q_o^* \ell}{\omega_R^2} \right) \left[M_{ii} \right]^{-1} [Q(k, M_o)] \right] \eta = \left(\frac{\omega}{\omega_R} \right)^2 \eta \tag{58}$$

in which $\delta = \frac{q_o}{q_\delta^*}$ is a dynamic pressure ratio, the ω_i are the natural frequencies of the K - M system

and ω, η are the eigenvalue and eigenvector of the system respectively. Since the evaluation of Q requires a priori knowledge of the flutter frequency, the eigenvalue problem cannot be solved directly. Several iteration schemes have appeared in the literature, the method for the determination of flutter eigensolutions employed in this work being as follows:

For a given Mach number, compute $Q(k, M_o)$ for a range of reduced frequencies, k. Since the elements Q_{ij} vary smoothly with k, each Q_{ij} can be approximated by a power series/spline fit over a chosen range of k, as

$$Q_{ij}(k) = \sum_{n=o}^{\bar{N}} \tilde{Q}_{ij,n} k^n \tag{59}$$

For a given Mach Number, the variables in Eqn. (58) are the density ρ and the speed of sound a_o. Generally, the relation between ρ and a_o is given in the form of standard atmospheric tables or tunnel operating characteristics, effectively reducing the unknowns to one variable, say ρ. Rewrite the definitions of dynamic pressure and reduced frequency in terms of Mach number as

$$q_o = \frac{1}{2}\rho U^2 = \frac{1}{2}\rho M_o^2 a_o^2 = \frac{\rho_o^* a_o^{*2} M_o^2}{2} \cdot \delta \tag{60}$$

and

$$k = \frac{\omega \ell}{U} = \frac{\omega \ell}{M_o a_o} \tag{61}$$

The iterative flutter solution in the atmospheric flight condition begins with the assumption of a low density ρ and the corresponding speed of sound a_o. Assuming some starting value of $\omega = \omega_R$, k and δ are then determinable. For this k, Q_{ij}'s are interpolated. With these quantities all the eigenvalues of Eqn. (58) are determined. Since Q is complex, the eigenvalues are generally complex, with their imaginary parts positive for decaying motion, which is inconsistent with the harmonic motion assumed. In order to determine consistent results, density is now increased and the above process repeated until one or more of the imaginary parts of ω change sign from positive to negative. The reduced frequency 'k' is then recomputed using the smallest real part of ω which has a negative imaginary part. The density ρ is then interpolated between those values of ρ which yield positive and negative imaginary parts of ω to obtain acceptable convergence to zero of the imaginary part of 'ω'. In practice rapid convergence to a real reduced frequency is obtained since the flutter formulation given by Eqn. (58) is generally not sensitive to small changes in k. In most cases linearly interpolated values of ρ are adequate for determination of the critical value. The critical dynamic pressure q_{ocr}, critical flight speed U_{cr}, and the flutter frequency ω_f are finally determined. A typical flow chart is presented in Figure 13.

Presentation of the flutter boundary in the current examples is in terms of the conventional stiffness-altitude parameter, $\frac{V}{\omega_R \ell} \cdot \frac{1}{\sqrt{\mu}}$ where μ, the ratio of structural mass to air mass is chosen by the user.

RESULTS AND DISCUSSION

The numerical results presented in this section have been obtained from two independent programs developed for isolated and interfering cases.

The characteristics of and parameters related to the various results are summarized in Table 1.

Isolated Wings

Aerodynamics for Isolated Wings

The accuracy of any unsteady aerodynamic method is critically illustrated by comparison of velocity potentials. Figures 3 to 5 compare the velocity potential distribution for a cropped delta wing with a low subsonic-leading edge at $M_o = 1.054$ for steady and oscillatory cases. Five consistent triangular elements compare very well with 30-box results from Reference 12. For the same cropped delta wing, generalized aerodynamic coefficients are presented for heave and pitch about a mid-chord axis at Mach numbers 1.118 and 1.201, in Table 2 and Figure 6. For such low Mach numbers and so few elements, the generalized coefficients deduced from the present method are in encouragingly good agreement with Reference 12 with the exception of moments due to pitching.

Table 3 shows the generalized coefficients for a rectangular wing of aspect ratio 2.0 at $M_o = 2.0$ in heave and pitch motion with $k = 0.3$, and in steady flow at $M_o = 1.2$. These have been compared with References 19 and 11, respectively. Vector plots of generalized forces are presented in Figure 7 and show generally good agreement.

The next example considers an AGARD swept wing of aspect ratio 1.45. The wing motions considered are heave, pitching about center chord, quadratic bending in the chordwise direction and quadratic bending in the spanwise direction, at two Mach numbers and two frequencies in each case. Comparisons have been made with Reference 20 which uses 30 to 40 characteristic boxes and Reference 19 which uses 17 chordwise Mach boxes whereas the present method uses only six triangles. Table 4 shows the generalized coefficients for $M_o = 1.2$, $k = 0.5$. For the first three modes good agreement has been obtained with References 20 and 19 while the fourth mode compares well with Reference 20 only. It appears that the Mach box results in Reference 19 are wrong or inaccurate for this mode. Table 5 shows Q_{ij}'s at $M_o = 1.2$, $k = 1.0$ for the same modes. Once again good agreement with Reference 20 is obtained.

Tables 6 and 7 show generalized coefficients at $M_o = 2.0$ for $k = 0.5$ and $k = 1.4$ respectively. Comparisons have been made again with References 19 and 20 in the former and with Reference 19 in the latter case. Results in Table 6 are in good agreement with Reference 20 but for the fourth mode (spanwise bending), again Reference 19 agrees with neither.

Flutter Solutions for Isolated Wings (NASA "HT-7" Example)

The basic purpose in the development of consistent aerodynamic forces is ultimately to improve the accuracy of aeroelastic solutions. Generalized forces have been used to determine the flutter boundary for a wing of aspect ratio 2.50 and taper ratio 0.3, known at NASA Langley as the HT-7 configuration. The leading edge sweepback angle is 50.5°. Mode shapes, generalized masses and natural frequencies are given in Reference 21. Flutter boundaries at $M_o = 1.3$, 1.573 and 1.64 were determined using the flutter equation (58). The altitude stiffness ratio $\frac{b_o \omega_2 \sqrt{\mu}}{a_o}$ and the flutter

TABLE 1
SUMMARY OF EXAMPLES

Cases	No.	Planform	Mach Number M_o	Reduced Frequency Parameter k	Data Presented	Comparisons Made with References	Figure/ Table Numbers
A. Isolated Wings	1	Cropped Delta	1.054	0.0	Velocity Potential	12	3/-
	2	Cropped Delta	1.054	1.05	Velocity Potential (Real)	12	4/-
	3	Cropped Delta	1.054	1.05	Velocity Potential (Imag)	12	5/-
	4	Cropped Delta	1.118, 1.201	1.05	Gen. Aero. Coefficients	12	6/2
	5	Rectangular Wing AR = 2.0	2.0 1.2	0.3 0.0	Gen. Aero. Coefficients	19 11	7/3
	6	AGARD Swept Wing AR = 1.45	1.2 1.2 2.0 2.0	0.5 1.0 0.5 1.4	Generalized Aerodynamic Coefficients	19,20 20 19,20 19	-/4 -/5 -/6 -/7
	7	NASA HT-7 Wing AR = 2.5	1.3 1.573 1.64	0.0 → 1.0	Flutter Boundary	21	8/-
B. Interfering Wings	1	Woodcock's Delta - Delta AR = 2.31 - 4.62	1.44	0.01	Damping Coefficients	22,24,29	9/-
	2	NASA 1A-2A Wings in Parallel AR = 6.8	1.45 1.60		Flutter Boundaries		11,12/-

TABLE 2
COMPARISON OF AERODYNAMIC GENERALIZED COEFFICIENTS Q_{ij}
FOR A CROPPED DELTA WING
$M_O = 1.118, 1.201$, $k = 1.05$ ($\bar{\omega} = 0.3$)
Modes: $q_1 = 2/7$, $q_2 = x - x_{mid\ chord}$

Method		Ref. 12		Present	
No. of ℄ Elements		30		6	
M_O	Qij	Real	Imaginary	Real	Imaginary
1.118	Q_{11}	0.0602	0.3163	0.0519	0.2849
	Q_{12}	1.1603	-0.0915	1.0811	-0.0452
	Q_{21}	-0.0504	-0.0746	-0.0353	-0.0390
	Q_{22}	-0.1631	0.3923	-0.0578	0.3039
1.201	Q_{11}	0.0646	0.2992	0.0560	0.2763
	Q_{12}	1.0727	-0.1159	1.0134	-0.0678
	Q_{21}	-0.0437	-0.0738	-0.0359	-0.0497
	Q_{22}	-0.1574	0.3684	-0.0847	0.3132

TABLE 3
COMPARISON OF AERODYNAMIC GENERALIZED COEFFICIENTS Q_{ij}
FOR RECTANGULAR WING OF ASPECT RATIO 2
$M_O = 2.0$, $k = 0.3$ and $M_O = 1.2$, $k = 0$
Modes: $q_1 = 1.0$, $q_2 = (x - c/2)$

Method		Mach Box		Ref. 19	Present	
No. of ℄ Elements		20			4	
M_O	k	Q_{ij}	Real	Imaginary	Real	Imaginary
2.0	0.3	Q_{11}	-0.191	-6.536	-0.217	-6.55
		Q_{12}	-21.87	-2.852	-22.07	2.56
		Q_{21}	-0.116	-3.072	-0.145	-3.18
		Q_{22}	-10.30	-1.929	-10.65	-1.75
Method		Mach Box		Ref. 11	Present	
No. of ℄ Elements		20			4	
M_O	k	Q_{ij}	Real	Imaginary	Real	Imaginary
1.2	0.0	Q_{12}	3.836		3.900	
		Q_{22}	-0.3783		-0.345	

TABLE 4

COMPARISON OF AERODYNAMIC GENERALIZED COEFFICIENTS Q_{ij} FOR AGARD SWEPT WING OF ASPECT RATIO 1.45

$M_o = 1.2, k = 0.5$

Modes: $q_1 = 1.0, q_2 = (x-c_r/2), q_3 = (x-c_r/2)^2, q_4 = y^2$

Method	Present		Mach Box Ref. 19		Char. Box Ref. 20	
No. of ℄ Elements	6		17		30+	
Q_{ij}	Real	Imaginary	Real	Imaginary	Real	Imaginary
Q_{11}	-0.0862	3.10	0.0119	3.473	-0.0228	3.3506
Q_{12}	3.46	2.18	3.801	1.681	3.671	1.7325
Q_{13}	3.6	-1.69	3.532	-1.185	3.353	-1.9538
Q_{14}	0.0357	0.766	-0.0894	0.702	0.0319	0.7478
Q_{21}	-0.32	0.13	-0.2695	-0.016	-0.2832	0.0083
Q_{22}	0.37	2.53	0.227	2.475	0.244	2.459
Q_{23}	2.58	-1.11	2.852	-1.055	2.703	-1.0507
Q_{24}	-0.0359	0.108	-0.0983	0.022	-0.0216	0.0764
Q_{31}	-0.194	0.5525	-0.1474	0.589	-0.164	0.5532
Q_{32}	0.68	1.45	0.7242	1.276	0.6824	1.305
Q_{33}	1.4	-0.312	1.444	-0.226	1.357	-0.2489
Q_{34}	0.0272	0.0985	-0.0692	0.064	-0.0182	0.0827
Q_{41}	-0.1135	0.723	-0.3301	-0.388	-0.0223	0.8380
Q_{42}	0.82	1.00	-0.3376	1.627	0.9066	0.574
Q_{43}	1.1	-0.386	0.6071	-0.151	0.9925	-0.1059
Q_{44}	-0.0432	0.232	-0.0978	-0.111	-0.018	0.2528

TABLE 5

COMPARISON OF AERODYNAMIC GENERALIZED COEFFICIENTS Q_{ij} FOR AGARD SWEPT WING OF ASPECT RATIO 1.45

$M_O = 1.2, k = 1.0$

Modes: $q_1 = 1.0, q_2 = (x-c_r/2), q_3 = (x-c_r/2)^2, q_4 = y^2$

Method	Present		Char. Box Ref. 20	
No. of ℓ Elements	6		30+	
Q_{ij}	Real	Imaginary	Real	Imaginary
Q_{11}	-0.565	3.52	-0.4042	3.5477
Q_{12}	4.12	1.804	4.0734	1.5832
Q_{13}	2.6	-0.081	2.56717	0.15633
Q_{14}	-0.159	0.785	-0.13087	0.72916
Q_{21}	-0.724	0.735	-0.70852	0.50164
Q_{22}	0.988	1.684	0.8165	1.73847
Q_{23}	2.082	0.192	2.21076	0.09960
Q_{24}	-0.216	0.212	-0.17584	0.13608
Q_{31}	-0.376	0.888	-0.33974	0.80848
Q_{32}	0.962	0.93	0.91061	0.8632
Q_{33}	1.238	0.454	1.19235	0.43602
Q_{34}	-0.153	0.18	-0.12188	0.12959
Q_{41}	-0.322	0.960	-0.145	0.89538
Q_{42}	0.719	0.808	0.97682	0.52965
Q_{43}	0.808	0.139	0.82489	0.23027
Q_{44}	-0.196	0.297	-0.13382	0.26639

TABLE 6
COMPARISON OF AERODYNAMIC GENERALIZED COEFFICIENTS Q_{ij}
FOR AGARD SWEPT WING OF ASPECT RATIO 1.45
$M_O = 2.0, k = 0.5$, Modes: $q_1 = 1.0$, $q_2 = (x - c_r/2)$, $q_3 = (x - c_r/2)^2$, $q_4 = y^2$

Method	Present		Mach Box Ref. 19		Characteristic Box Ref. 18	
No. of ℄ Elements	6		17+		40	
Q_{ij}	Real	Imaginary	Real	Imaginary	Real	Imaginary
Q_{11}	0.0698	2.6047	0.06007	2.565	0.05999	2.52563
Q_{12}	2.6094	0.4950	2.572	0.5374	2.53299	0.51324
Q_{13}	1.5535	0.6932	1.566	0.6912	1.51857	0.65485
Q_{14}	-0.0121	0.6462	-0.01934	0.5779	-0.01374	0.57410
Q_{21}	-0.0057	0.4767	-0.001025	0.4388	-0.00307	0.44491
Q_{22}	0.4913	0.7677	0.45666	0.7695	0.46181	0.75181
Q_{23}	1.4937	0.2990	1.533	0.2829	1.48154	0.27395
Q_{24}	-0.0230	0.1655	-0.02136	0.01302	-0.01853	0.14258
Q_{31}	-0.0095	0.5410	-0.00299	0.5293	-0.00676	0.50594
Q_{32}	0.5482	0.4688	0.5422	0.4457	0.51692	0.44825
Q_{33}	0.8621	0.3366	0.8699	0.3102	0.84474	0.30134
Q_{34}	-0.0234	0.1133	-0.01891	0.1028	-0.01730	0.10143
Q_{41}	0.0186	0.7421	-0.1180	-0.1415	0.01719	0.67412
Q_{42}	0.7319	0.2103	-0.1348	0.6712	0.66558	0.19623
Q_{43}	0.5752	0.3510	0.3856	0.07844	0.53698	0.32057
Q_{44}	-0.0224	0.2793	-0.05113	-0.03105	-0.01956	0.23862

TABLE 7

COMPARISON OF AERODYNAMIC GENERALIZED COEFFICIENTS Q_{ij} FOR AGARD SWEPT WING OF ASPECT RATIO 1.45

$M_O = 2.0, k = 1.4$

Modes: $q_1 = 1.0, q_2 = (x\text{-}c_r/2), q_3 = (x\text{-}c_r/2)^2, q_4 = y^2$

Method	Present		Mach Box Ref. 19	
No. of ℄ Elements	6		17	
Q_{ij}	Real	Imaginary	Real	Imaginary
Q_{11}	-0.060	2.4	-0.1529	2.35
Q_{12}	2.550	0.77	2.5010	0.8112
Q_{13}	1.511	0.556	1.480	0.5726
Q_{14}	-0.134	0.666	-0.1862	0.6014
Q_{21}	-0.336	0.484	-0.3306	0.4262
Q_{22}	0.625	0.856	0.5708	0.8512
Q_{23}	1.356	0.28	1.357	0.2858
Q_{24}	-0.179	0.218	-0.1774	0.1791
Q_{31}	-0.258	0.574	-0.2473	0.5411
Q_{32}	0.647	0.517	0.6291	0.4906
Q_{33}	0.766	0.334	0.7360	0.3294
Q_{34}	-0.167	0.172	-0.1496	0.1413
Q_{41}	-0.488	0.682	-0.7363	0.1362
Q_{42}	0.665	0.328	0.1201	0.5232
Q_{43}	0.625	0.271	0.2283	0.1796
Q_{44}	-0.155	0.332	-0.3423	0.00649

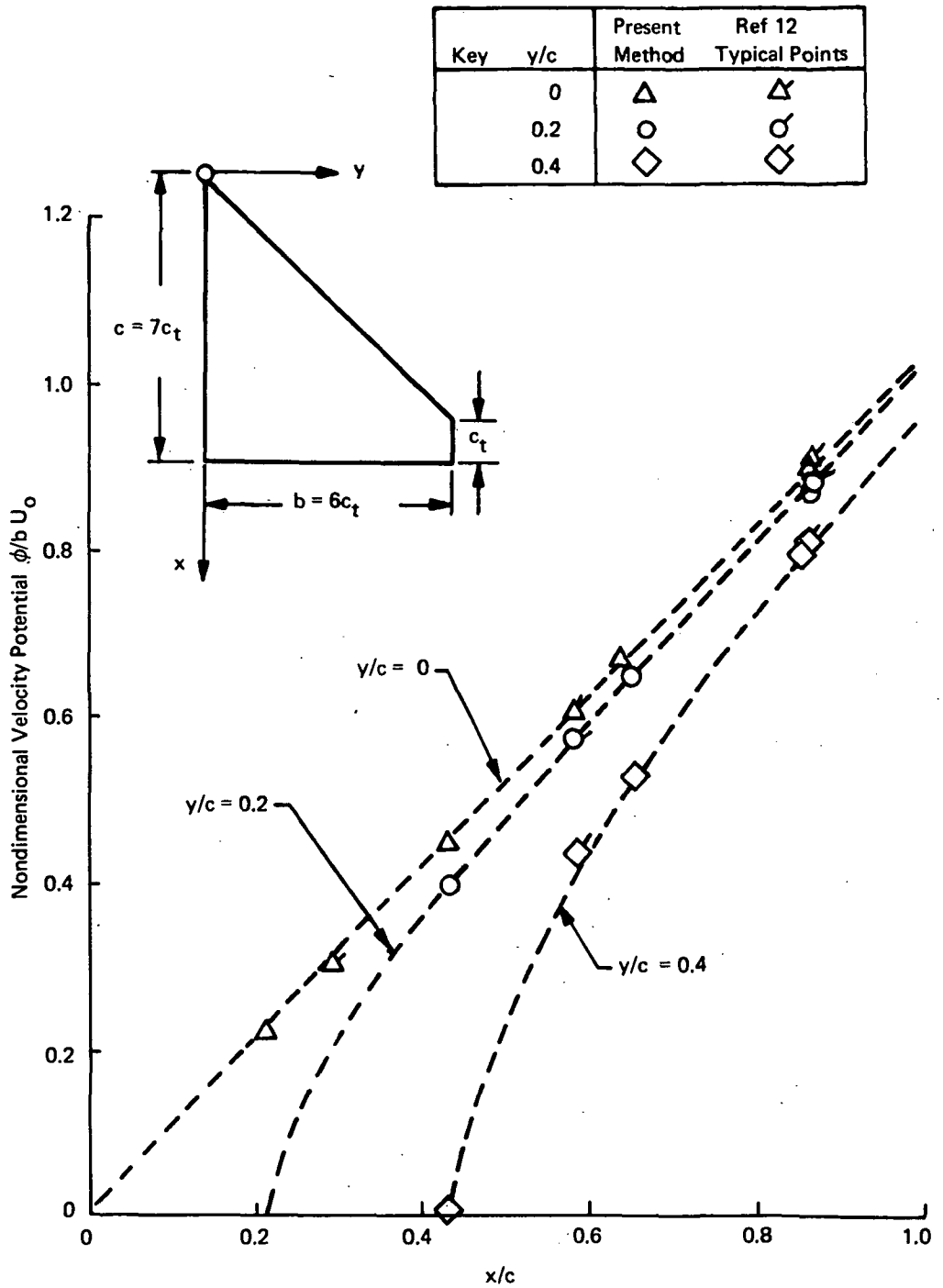

Figure 3. Velocity Potential Distribution on a Cropped Delta Wing at Constant Incidence $M_o = 1.054$, $k = 0.0$

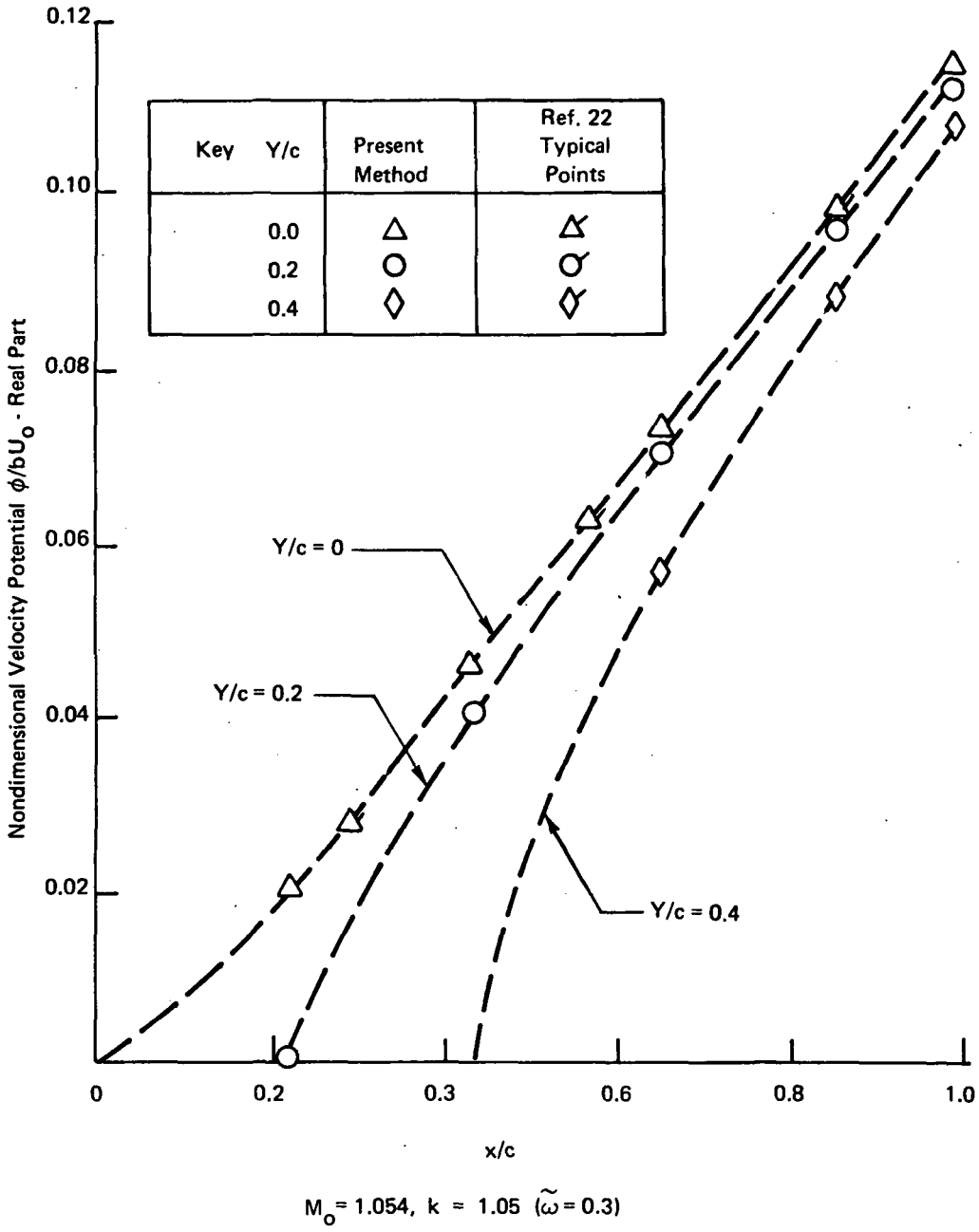

Figure 4. Real Part of Velocity Potential on a Cropped Delta Wing In Translation

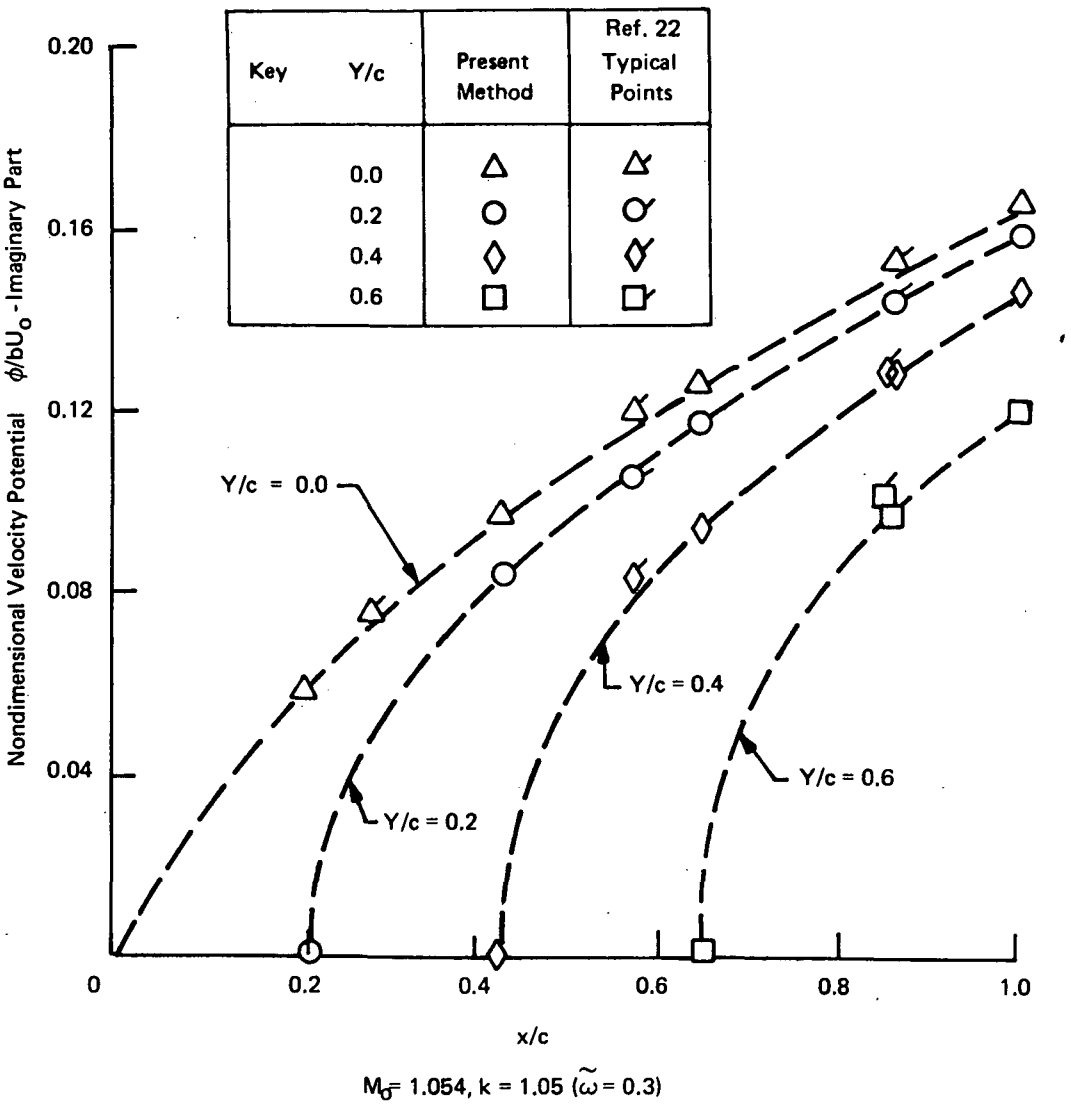

Figure 5. Imaginary Part of Velocity Potential on a Cropped Delta Wing In Translation

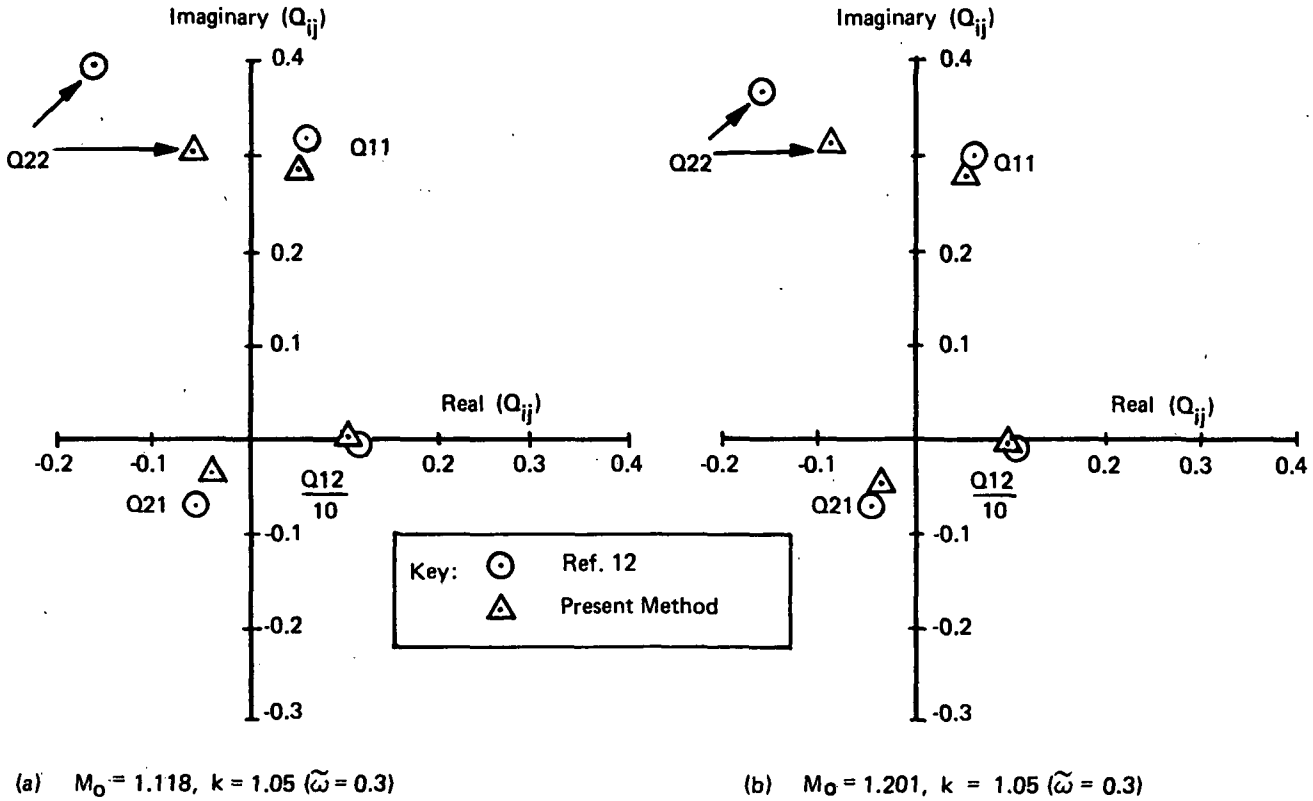

Figure 6. Vector Plot of Aerodynamic Generalized Coefficients Q_{ij} for a Cropped Delta Wing

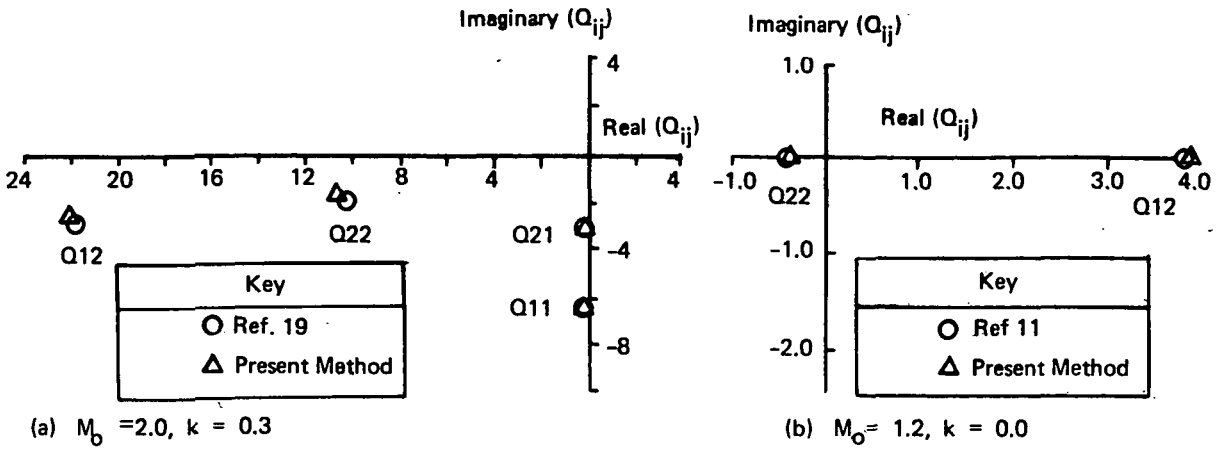

Figure 7. Vector Plot of Aerodynamic Generalized Coefficients Q_{ij} for a Rectangular Wing of Aspect Ratio 2

to reference frequency ratio (ω/ω_2) are shown in Figure 8. Solutions obtained from supersonic kernel function and piston theories (Reference 21) are also shown for subsonic leading edge and supersonic leading edge cases respectively. The flutter boundary from the kernel function theory at a Mach number of 1.573 yields a conservative result while the piston theory is unconservative. The flutter boundary obtained from the consistent approach lies in between these two results, encouragingly close to the experimental flutter point. In the subsonic leading edge case, the present method gives a frequency ratio very close to the kernel function approach. In the supersonic leading edge case it suggests a transition toward piston theory solution. The experimental flutter frequency is lower than from the present solution.

Interfering Wings

Two sets of computations were made using the program for interfering wings. The first example was that considered by Woodcock and York in Reference 22. (See Figure 9.) The second (NASA example) was a combination of two tapered wings of aspect ratio 6.8 and leading edge sweep of 16.0°. (see Figure 10.) No experimental comparisons were available for this latter case. However, flutter calculations have been carried out to illustrate the effect of separation distance at two Mach numbers. Additionally, the effect of static deformation on flutter has been roughly assessed at one Mach number.

Generalized Aerodynamics (Interfering Wing-Tail Example)

The reference 22 wing-tail combination is shown in Figure 9. The aspect ratios of wing and tail are 2.31 and 4.62 respectively, the tail span being half the wing span. The apex of the tail is situated at $\bar{x} = 2\sqrt{3}$ and $\bar{z} = 0.5$, which corresponds to d = 0.866 and z = 0.5 in Reference 22. The number of elements used in Reference 22 and in the present analysis are respectively, 300 on the wing with 50 on the tail, and 49 on the wing with 16 on the tail.

Computations were made at a Mach number of 1.44 for which the wing leading edge is subsonic and the tail leading edge is supersonic. The modes are heave and pitch of the whole configuration and heave and pitch of the tail alone, the pitch axis in both cases being located at 2/3 of wing root chord. The computation was performed at a reduced frequency of k = 0.01 as in Reference 22.

In order to give a rough indication of some of the interference effects, a few heave damping coefficients for the wing alone and tail alone are quoted from the present work, and References 22 and 23.

Results are presented in Table 8 together with corresponding figures from Reference 22, and some comparable results from Reference 24 for $\bar{z} = 0$.

No objective comments are offered at this stage except that generally comparable results are obtained for coefficients of significance.

Flutter of Interfering NASA Wings

The two wings considered are of identical planform with zero stagger (See Figure 10). Aspect and taper ratios are 6.8 and 0.364 respectively, and the leading edge sweep is 16°.

Flutter calculations were performed at Mach numbers of 1.45 and 1.60 for various separation distances including no interference. The results are presented in two forms on Figures 11 and 12, as

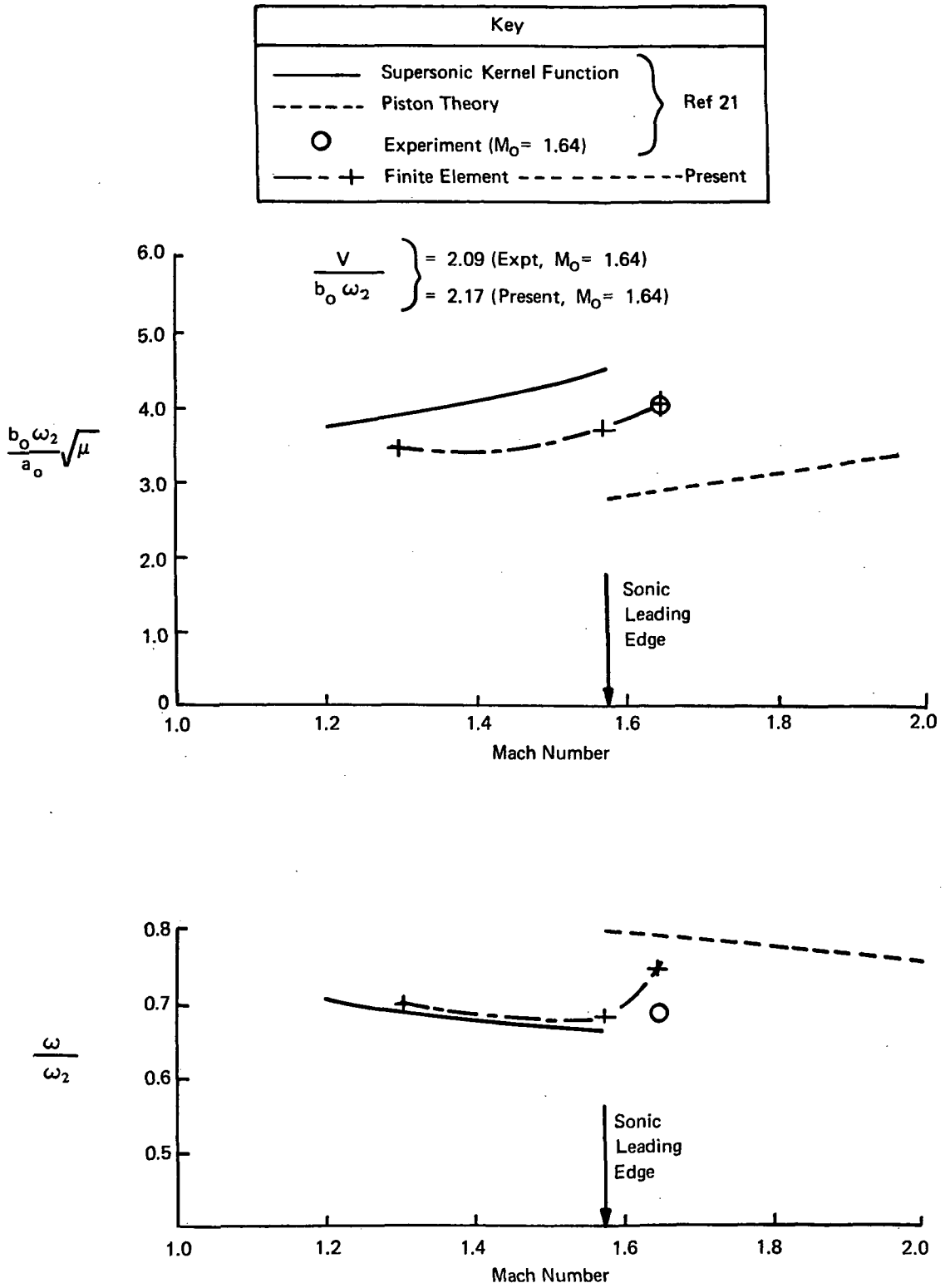

Figure 8. Flutter Boundary in Terms of the Stiffness - Altitude Parameter and Ratio of Flutter Frequency to the Second Natural Frequency versus M for HT-7 Wing

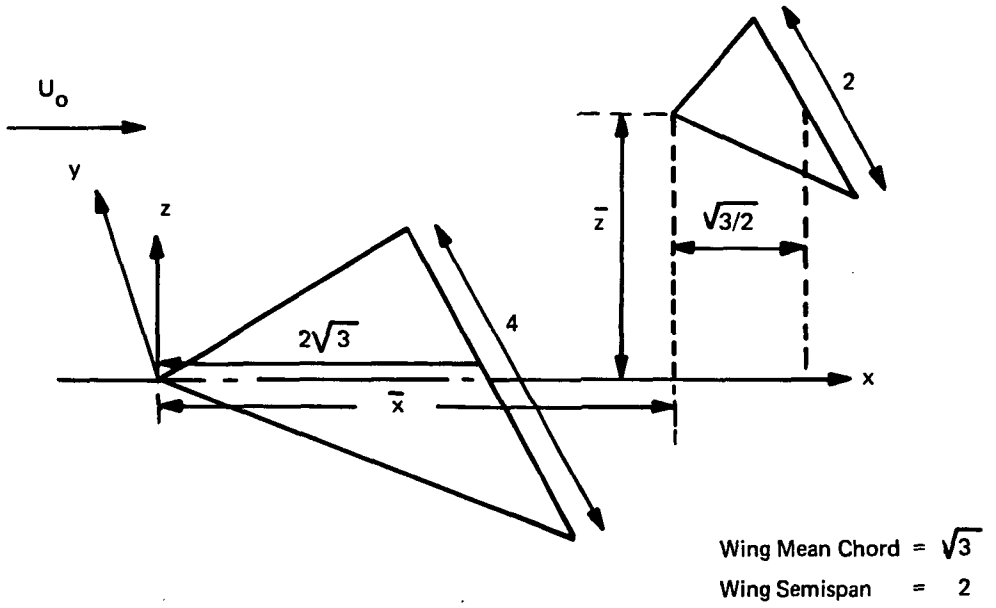

Figure 9. Configuration of Triangular Wing – Tailplane

TABLE 8

COMPARISON OF Im. PART OF GENERALIZED DAMPING COEFFICIENTS Q_{ij} FOR DELTA WING COMBINATION AT $M_o = 1.44$, $k = 0.01$

Modes 1 - Heave of Wing and Tail
2 - Pitch of Wing and Tail
3 - Heave, Tail Only
4 - Pitch, Tail Only

Method		Present	Ref. 22	Ref. 24	Ref. 29
Total No. of Elements		Wing 49 Tail 16	Wing 300 Tail 50	–	
Im	Q_{ij} \ $\bar{z}$	0.5	0.5	0.0	
	Q_{11}	2.6466 (2.180*)	2.954 (2.820*)	3.06	(2.58*)
	Q_{12}	0.6670	0.170	0.37	
	Q_{13}	0.3695	0.477		
	Q_{14}	0.2850	0.387		
	Q_{21}	0.4280	0.171	0.21	
	Q_{22}	1.1740	0.934	1.70	
	Q_{23}	0.3741	0.483		
	Q_{24}	0.2920	0.395		
	Q_{31}	0.4020	0.148		
	Q_{32}	0.6667	0.343		
	Q_{33}	0.3696	0.477		
	Q_{34}	0.2850	0.387		
	Q_{41}	0.388	0.155		
	Q_{42}	0.664	0.358		
	Q_{43}	0.374	0.483		
	Q_{44}	0.292	0.395		

*Wing Alone in Heave

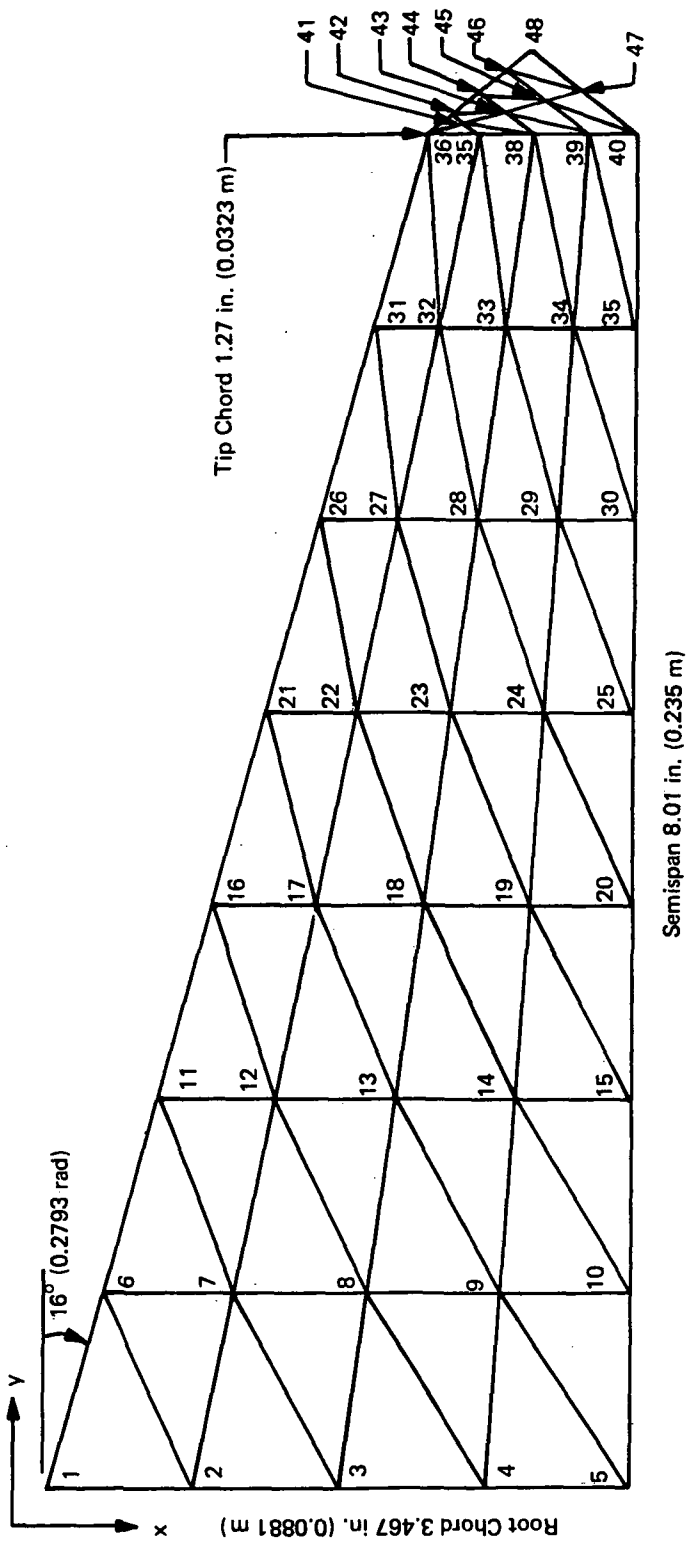

Figure 10. NASA 1A and 2A Configuration and M_O = 1.6 Aero Grid

flutter speed against separation for two Mach numbers, and flutter speed against Mach number for various separation distances. Additionally at $M_o = 1.60$ only, the effect on flutter speeds of deflection due to thickness loading was assessed roughly. This was done by first determining the flutter dynamic pressure for zero thickness. At this dynamic pressure the steady interference loading due to thickness was determined and applied to the wings to determine their approximate deflected equilibrium positions. Flutter calculations were then repeated for these deflected positions by recomputing zero-thickness generalized forces, etc.

Modal data for unit generalized masses of the two wings are given in Tables 9A and 9B for the first four modes of each wing, these being the modes used in the flutter calculation.

Figure 11 shows the effect of separation on reduced flutter speed at $M_o = 1.45$ and 1.60, for which asymptotic flutter speeds without interference are 1.77 and 1.87 respectively. At $M_o = 1.45$, interference commences at the root at a dimensionless separation of 0.95 and has spread to the tip at a separation of 0.348. At $M_o = 1.60$, the separations are 0.80 for the root and 0.293 for the tip interference.

The results for $M_o = 1.60$ suggest that the effect of interference, which starts at the root, is first small, as might be expected. As the inteference effect reaches beyond mid-span, the flutter speed falls much more rapidly, the rate of fall decreasing again as the interference effect spreads out to the tip. The same general conclusions hold for $M_o = 1.45$. However, at this Mach number the total reduction in flutter speed is more drastic and is probably affected by the shortcomings of linearized theory which predicts negative two-dimensional aerodynamic damping for a range of reduced frequency below $M_o = \sqrt{2}$. The wings in the present example are not too far removed from the unswept two-dimensional case.

Figure 12 crossplots flutter speed against Mach number and also sketches the asymptotic non-interference boundary.

Both Figures 11 and 12 include the effect on flutter speed at $M_o = 1.6$ of the static interference. The effect is small and the single iteration used for static deflection is probably adequate. This effect has not been determined for $M_o = 1.45$.

An interesting feature of the flutter modal vector behavior was noticed as the separation decreased. Without interference, the thinner, lower frequency Wing 1A fluttered at a lower reduced speed than Wing 2A (i.e., at 1.87 and 1.77 for Mach numbers of 1.60 and 1.45 respectively –see Figure 11). The flutter mode was dominated by Mode 3, its first torsion mode.

However, for the smallest separation case ($\frac{Z}{2b} = 0.214$) of the Mach 1.60 calculations, the flutter mode and frequency were dominated by the thicker wing 2A. The flutter frequency was 2837 rps compared to the zero airspeed Wing 2A Mode 3 (torsion) frequency of 2819 rps.

The significant contributions to the modal vector were:

Wing 1A	- Mode 3 (first torsion)	+ 0.080
Wing 2A	- Mode 1 (first bending)	- 0.083
	Mode 3 (first torsion)	+ 0.928.

TABLE 9A
MODE SHAPES AND FREQUENCIES FOR NASA WING MODEL 1A

Mode	1	2	3	4
Frequency	346.0.rps	1290.0.rps	2121.4 rps	3169.0 rps
Grid Point	–	–	–	–
1	0.0	0.0	0.0	0.0
2	-0.248374E 00	0.846053E 00	0.340652E 00	0.156274E 01
3	0.0	0.0	0.0	0.0
4	-0.661762E 00	-0.132569E 01	-0.162827E 02	-0.955371E 01
5	-0.148843E 01	-0.574492E 01	-0.501730E 02	-0.306777E 02
6	0.373210E 01	-0.110920E 02	0.256854E 02	-0.238349E 02
7	0.510167E 01	-0.151072E 02	0.166748E 02	-0.290629E 02
8	0.600098E 01	-0.188923E 02	-0.383127E 01	-0.338759E 02
9	0.714894E 01	-0.260340E 02	-0.358998E 02	-0.482695E 02
10	0.751287E 01	-0.329570E 02	-0.752936E 02	-0.650456E 02
11	0.144421E 02	-0.377111E 02	0.664367E 02	-0.624758E 02
12	0.168970E 02	-0.433420E 02	0.358953E 02	-0.625167E 02
13	0.189125E 02	-0.494378E 02	-0.280577E 01	-0.635001E 02
14	0.202884E 02	-0.557970E 02	-0.480677E 02	-0.659036E 02
15	0.210618E 02	-0.629261E 02	-0.969772E 02	-0.717563E 02
16	0.327125E 02	-0.656615E 02	0.107401E 03	-0.631332E 02
17	0.356679E 02	-0.688935E 02	0.594811E 02	-0.503386E 02
18	0.380185E 02	-0.728230E 02	0.537178E 01	-0.379178E 02
19	0.397843E 02	-0.779427E 02	-0.530814E 02	-0.274941E 02
20	0.409142E 02	-0.844757E 02	-0.113283E 03	-0.197513E 02
21	0.584188E 02	-0.713794E 02	0.142117E 03	-0.106175E 01
22	0.614552E 02	-0.701302E 02	0.804984E 02	0.196408E 02
23	0.639868E 02	-0.705903E 02	0.145253E 02	0.402410E 02
24	0.659998E 02	-0.730238E 02	-0.541276E 02	0.602483E 02
25	0.674978E 02	-0.777540E 02	-0.123549E 03	0.794476E 02
26	0.912201E 02	-0.310397E 02	0.158395E 03	0.598651E 02
27	0.940856E 02	-0.257317E 02	0.883828E 02	0.758822E 02
28	0.965729E 02	-0.226300E 02	0.157768E 02	0.941429E 02
29	0.986789E 02	-0.219322E 02	-0.581623E 02	0.114858E 03
30	0.100418E 03	-0.237869E 02	-0.132125E 03	0.138293E 03
31	0.129880E 03	0.676545E 02	0.144149E 03	-0.820722E 01
32	0.132357E 03	0.748086E 02	0.730007E 02	-0.304004E 01
33	0.134593E 03	0.798729E 02	0.785800E 00	0.718163E 01
34	0.136588E 03	0.827491E 02	-0.717218E 02	0.229209E 02
35	0.138360E 03	0.834467E 02	-0.143789E 03	0.443335E 02
36	0.171953E 03	0.210059E 03	0.989585E 02	-0.242098E 03
37	0.173924E 03	0.216496E 03	0.345747E 02	-0.241725E 03
38	0.175761E 03	0.221376E 03	-0.298829E 02	-0.235332E 03
39	0.177465E 03	0.224694E 03	-0.941044E 02	-0.222813E 03
40	0.179052E 03	0.226521E 03	-0.157824E 03	-0.204166E 03

TABLE 9B
MODE SHAPES AND FREQUENCIES FOR NASA WING MODEL 2A

Mode	1	2	3	4
Frequency	476.6 rps	1716.0 rps	2819 rps	4211 rps
Grid Points	–	–	–	–
1	0.0	0.0	0.0	0.0
2	-0.216321E 00	0.733357E 00	0.293900E 00	0.134361E 01
3	0.0	0.0	0.0	0.0
4	-0.576453E 00	-0.115600E 01	-0.141411E 02	-0.832933E 01
5	-0.129031E 01	-0.500474E 01	-0.435684E 02	-0.266567E 02
6	0.323887E 01	-0.962833E 01	0.222815E 02	-0.207137E 02
7	0.442801E 01	-0.131154E 02	0.144487E 02	-0.252496E 02
8	0.520807E 01	-0.163985E 02	-0.333866E 01	-0.294104E 02
9	0.620506E 01	-0.225997E 02	-0.311611E 02	-0.418901E 02
10	0.652201E 01	-0.286114E 02	-0.653320E 02	-0.564257E 02
11	0.125306E 02	-0.327159E 02	0.576116E 02	-0.542299E 02
12	0.146600E 02	-0.375993E 02	0.311273E 02	-0.542434E 02
13	0.164083E 02	-0.428873E 02	-0.244496E 01	-0.550728E 02
14	0.176038E 02	-0.484108E 02	-0.417061E 02	-0.571416E 02
15	0.182764E 02	-0.546015E 02	-0.841242E 02	-0.621955E 02
16	0.283770E 02	-0.569429E 02	0.931467E 02	-0.547628E 02
17	0.309410E 02	-0.597486E 02	0.515929E 02	-0.436474E 02
18	0.329810E 02	-0.631616E 02	0.466318E 01	-0.328564E 02
19	0.345137E 02	-0.676064E 02	-0.460318E 02	-0.237896E 02
20	0.354956E 02	-0.732784E 02	-0.982352E 02	-0.170476E 02
21	0.506714E 02	-0.618871E 02	0.123267E 03	-0.918818E 00
22	0.533058E 02	-0.608072E 02	0.698350E 02	0.170479E 02
23	0.555023E 02	-0.612102E 02	0.126208E 02	0.349313E 02
24	0.572493E 02	-0.633248E 02	-0.469159E 02	0.523054E 02
25	0.585499E 02	-0.674306E 02	-0.107110E 03	0.689820E 02
26	0.791174E 02	-0.268896E 02	0.137385E 03	0.518804E 02
27	0.816033E 02	-0.222904E 02	0.766725E 02	0.657801E 02
28	0.837612E 02	-0.196051E 02	0.137075E 02	0.816333E 02
29	0.855884E 02	-0.190043E 02	-0.504115E 02	0.996200E 02
30	0.870982E 02	-0.206159E 02	-0.114543E 03	0.119965E 03
31	0.112643E 03	0.587043E 02	0.125004E 03	-0.721169E 01
32	0.114791E 03	0.649023E 02	0.633012E 02	-0.270577E 01
33	0.116731E 03	0.692881E 02	0.672285E 00	0.618898E 01
34	0.118462E 03	0.717767E 02	-0.662088E 02	0.198692E 02
35	0.119999E 03	0.723772E 02	-0.124703E 03	0.384641E 02
36	0.149126E 03	0.182181E 03	0.857724E 02	-0.210011E 03
37	0.150836E 03	0.187757E 03	0.299216E 02	-0.209643E 03
38	0.152429E 03	0.191982E 03	-0.259948E 02	-0.204055E 03
39	0.153908E 03	0.194855E 03	-0.817059E 02	-0.193157E 03
40	0.155284E 03	0.196436E 03	-0.136979E 03	-0.176952E 03

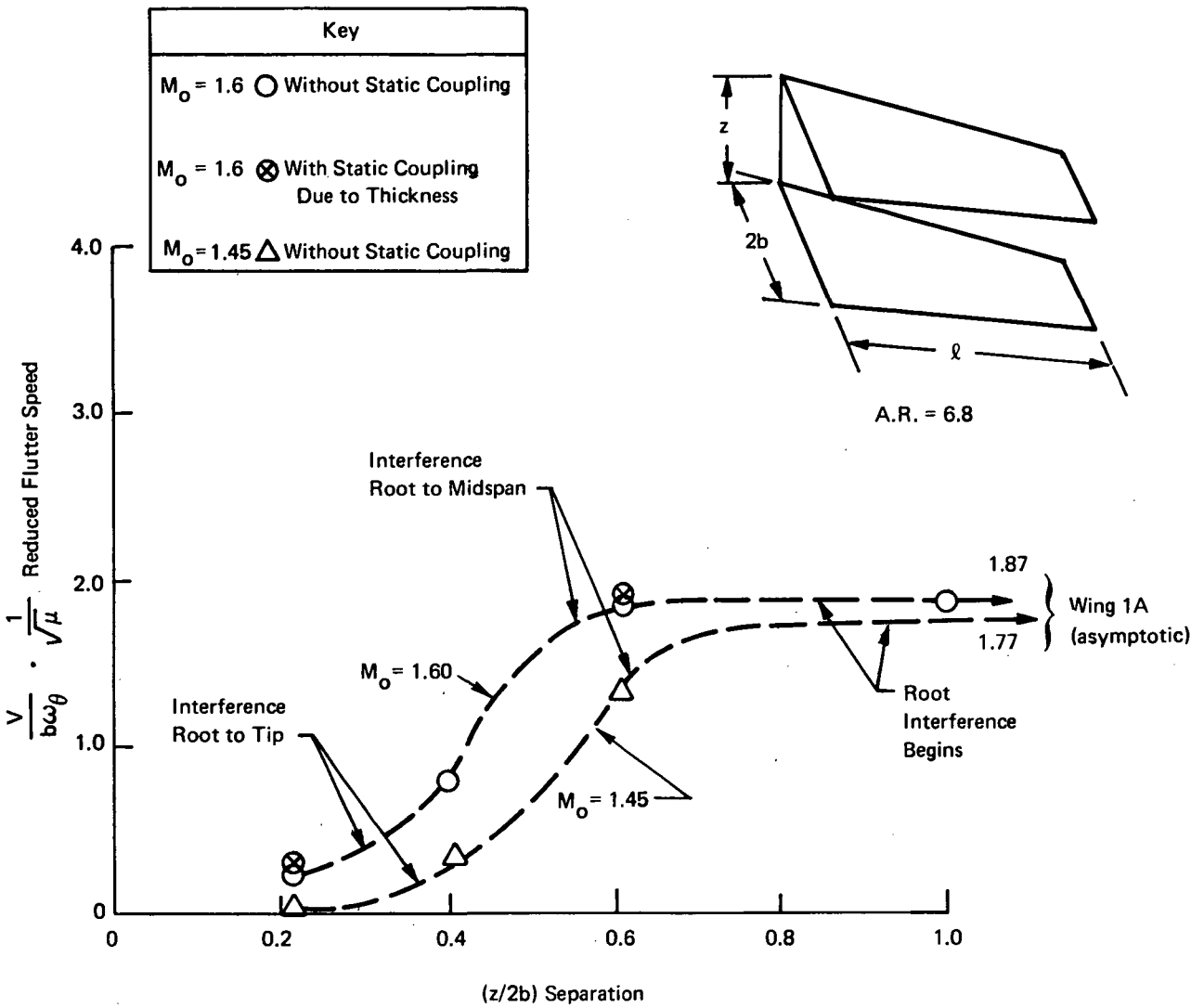

Figure 11. Variation of Reduced Flutter Speed with Vertical Separation at M_o = 1.45 and M_o = 1.6

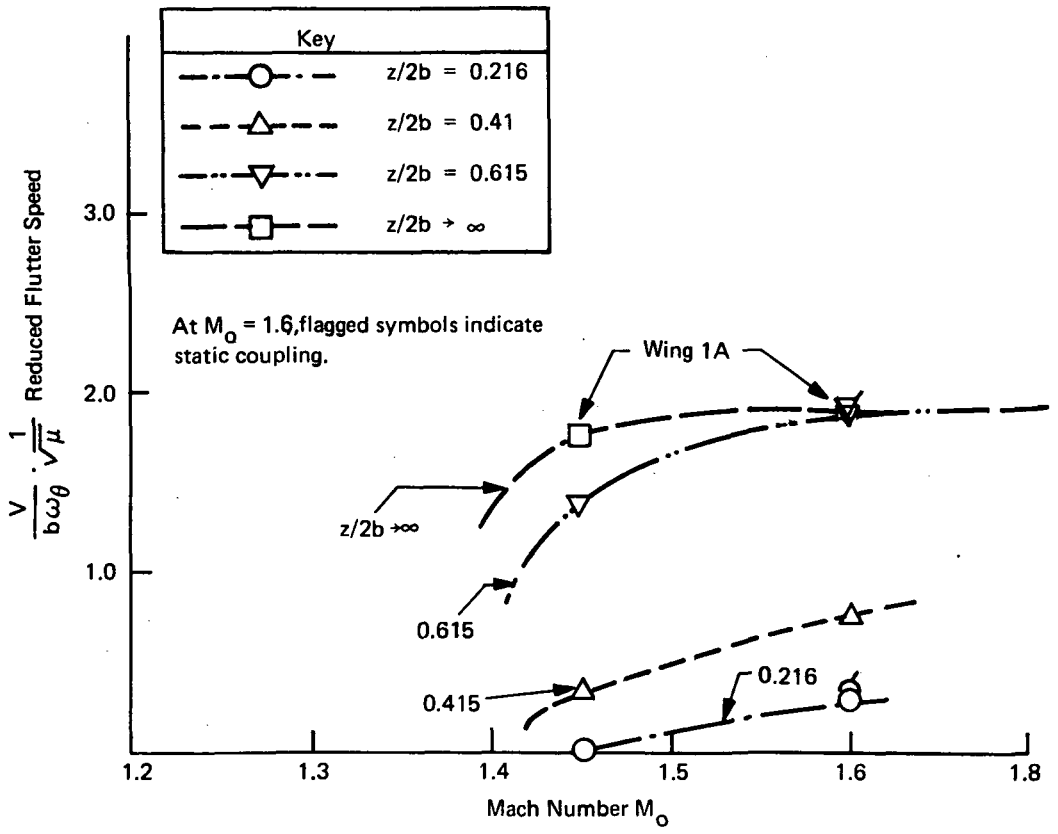

Figure 12. Variation of Reduced Flutter Speed with Vertical Separation (Cross-Plot of Figure 11)

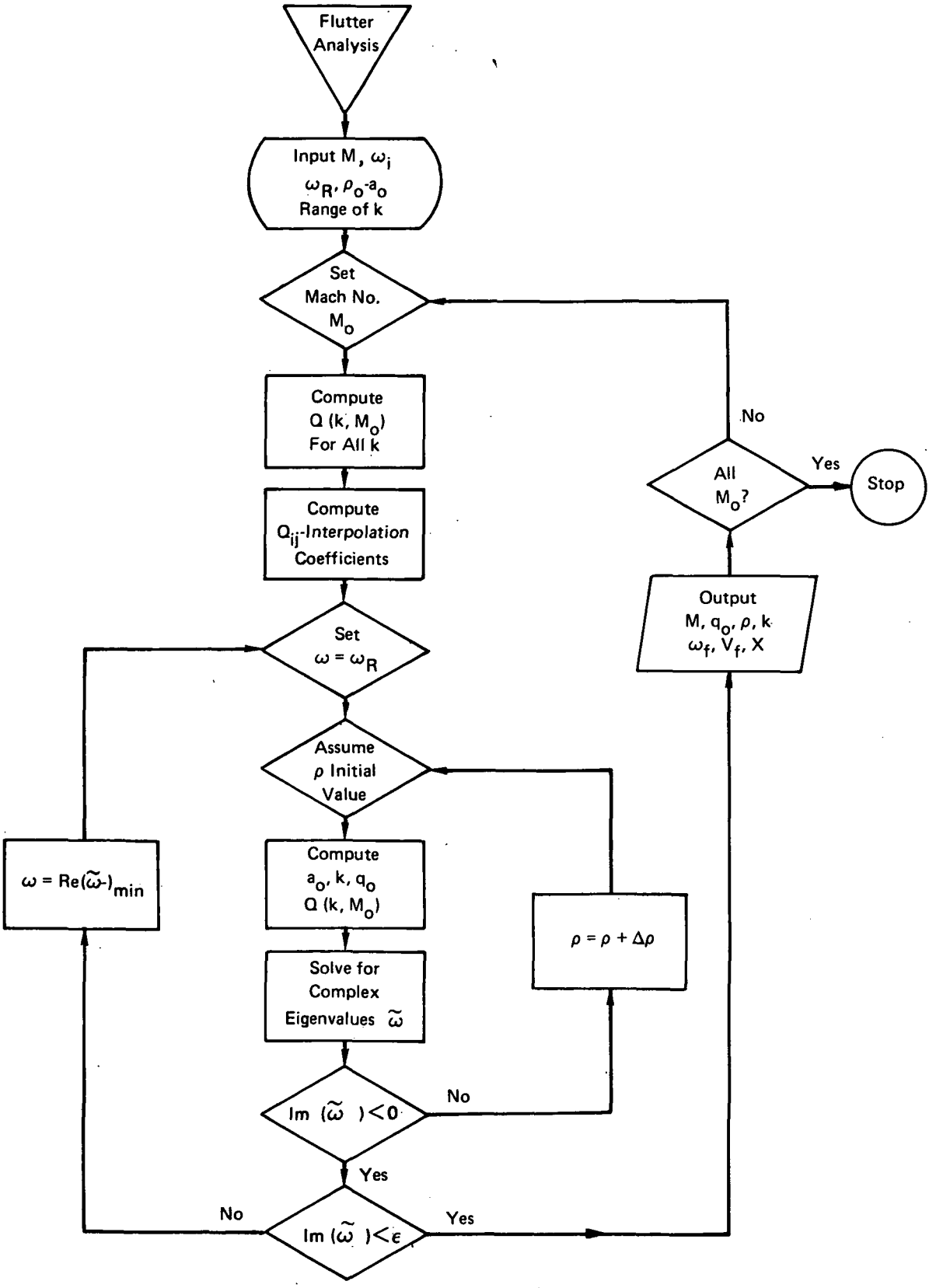

Figure 13. Flow Chart for Flutter Analysis

CONCLUSIONS AND RECOMMENDATIONS

Further applications of an improved consistent approach to the derivation of unsteady aerodynamic forces for planar wings have been illustrated, and an operational computer program produced. Similar techniques have been developed for nearly parallel interfering planar wings, and an operational program has been used for the study of flutter characteristics of a pair of wings as affected by separation and steady airload deflection effects.

In general terms, it appears that the approximations made in satisfying boundary conditions for interfering wings are warranted for the limited range of applications considered, but further evidence of their validity should be obtained as more comparative numerical examples become available.

The encouraging comparisons with References 11, 12, 19 and 20 confirm general conclusions concerning the advantages of the present approach in reducing the numerical size of matrix equations necessary for acceptable accuracy.

With respect to the excellent experimental flutter correlation obtained in Figure 8, the example stands alone and requires further applications before general conclusions are possible. The same remarks apply concerning the Kernel Function - Piston Theory transition noted in the text.

The interference algorithm has illustrated the probability of strong detrimental effects of proximity on the flutter of interfering wings.

The flutter algorithm used offers potential for more direct computer operator interaction than more common approaches and is worthy of additional development.

The present programs are not optimally designed from the computer time point of view, but have generally evolved with the developments reported. No computer time comparisons with Reference 22 are available, for example, but again, the marked difference in grid sizes is apparent.

The expansion of the present approach to include more complex interacting and interfering configurations, subsonic trailing edges and interfering wakes is feasible. It is probable that the present approach will be even more advantageous from the numerical point of view in these more complex circumstances. The basic method could additionally be reformulated in terms of an intergrated potential approach (References 25-27) avoiding the use of diaphragms.

An iterative form of static aeroelastic solution for deforming, interacting surfaces is feasible. In these problems, the domain of dependence of a particular point may alter significantly with the "static" deformation, and require an iterative type solution to the resulting equation. Flutter solutions could continue to be determined as linearized problems about the static equilibrium position.

APPENDIX

Derivation and numerical integration of the velocity potential and downwash matrices for basic triangular elements are described in this section. Details of the programming for the solution of the total problem are contained in Reference 28.

Velocity Potential - Isolated Wing

For thin wings in supersonic flow, the nondimensional source distribution due to perturbed motion from Eq. (26) is given by

$$\sigma(\Xi_i) = \frac{w(\Xi_i)}{U} = \left[\bar{\lambda}\,\Omega(\Xi) + \Omega_\xi\right] \rho_j \tag{A-1}$$

where the interpolation matrix $\Omega(\Xi_i)$ for the triangular element is

$$\Omega(\Xi) = \left[\xi, \eta, 1\right] T \tag{A-2}$$

$$\text{in which} \quad T = \begin{bmatrix} \xi_1 & \eta_1 & 1 \\ \xi_2 & \eta_2 & 1 \\ \xi_3 & \eta_3 & 1 \end{bmatrix}^{-1} \tag{A-3}$$

$$\text{and} \quad \Omega_\xi = \frac{\partial \Omega}{\partial \xi} = \begin{bmatrix} 1 & 0 & 0 \end{bmatrix} T \tag{A-4}$$

Using the source displacement relation given by Eqn. (A-1) in Eqn. (4), the velocity potential influence coefficient matrix relating nodal source strengths to nodal displacements can be written similar to Eqn. (11) as

$$\Phi_{ij} = \frac{1}{\pi} \iint_{S_j} F(X_i, \Xi_j) \left[\bar{\lambda}\,\Omega + \Omega_\xi\right] dS \tag{A-5}$$

(Note the distinctive definitions of Φ_{ij} for isolated and interfering wings).

Integration of Eqn. (A-5) is performed numerically using Gaussian 5-point quadrature coefficients. The elements cut by Mach lines emerging from the position X_i were truncated by a small width and integrated analytically using characteristic coordinates. More detailed information is contained in Reference 13.

Velocity Potential - Interfering Wings

For interfering wings the source distribution is not known until the kinematic boundary conditions as given by Eqn. (13) are satisfied. This requires the normal derivative of the velocity potential. When this is performed the kernel F in Eqn. (5) will exhibit a higher order singularity which usually requires more elaborate numerical integration. However, this situation can be avoided by using the equality credited to Watson (References 8 and 11),

$$\frac{\cos\left(\frac{\hat{k}}{M_o}\sqrt{\mu^2 - \nu^2}\right)}{\sqrt{\mu^2 - \nu^2}} = -\frac{\partial}{\partial \nu}\left(\psi(\mu, \nu)\right) \tag{A-6}$$

where $\mu^2 = (x - \xi)^2 - \beta^2 (z - \zeta)^2$

$\nu = \beta (y - \eta)$ (A-7)

$\hat{k} = \frac{kM_o^2}{\beta^2}$

$k = \frac{\omega \ell}{U}$ (A-8)

and $\psi(\mu, \nu) = J_o \left(\frac{\hat{k}}{M_o} \mu\right) \sin^{-1}\left(\frac{\nu}{\mu}\right)$

$$+ \sum_{r=1}^{\infty} \frac{(-1)^r}{r} J_{2r}\left(\frac{\hat{k}}{M_o}\mu\right) \sin\left(2r \sin^{-1}\left(\frac{\nu}{\mu}\right)\right) \quad \text{(A-9)}$$

in which J_{2r} is a Bessel function of even order.

Using (A-6) in Eq. (5) the velocity potential influence coefficient matrix from Eqn. (11) is given by

$$\Phi_{ij} = \frac{1}{\pi} \int_{\xi_\ell}^{\xi_u} e^{-i\hat{k}(x_i - \xi_j)} \int_{\eta_\ell}^{\eta_u} \Omega(\xi_j, \eta_j) \frac{\partial \psi}{\partial \nu} \partial\eta \, d\xi \quad \text{(A-10)}$$

Substituting from (A7) and (A8) and integrating by parts, the velocity potential becomes

$$\Phi_{ij} = -\frac{1}{\pi\beta} \int_{\xi_\ell}^{\xi_u} e^{-i\hat{k}(x_i - \xi_j)} \Big[\Omega(\xi, \eta_u) \psi(\xi, \eta_u) - \Omega(\xi, \eta_\ell) \psi(\xi, \eta_\ell) - \Omega_\eta \int_{\eta_\ell}^{\eta_u} \psi(\xi, \eta) \, d\eta \Big] \, d\xi \quad \text{(A-11)}$$

The upper and lower limits of η are given by

$\eta_u = a_u \xi + b_u$

$\eta_\ell = a_\ell \xi + b_\ell$ (A-12)

where a_u and a_ℓ are slopes of the upper and lower boundary lines, (i.e. line 1-3 and line 1-2 respectively) and b_u and b_ℓ are the corresponding constants (See Figure 14A). The initial position of each element is assumed to be the average of its z coordinates if the wing is not wholly parallel to the x - y plane. The integrand in Eq. (A11) is analytic in the fore Mach cone region and Gaussian type numerical integrations have been employed in all cases.

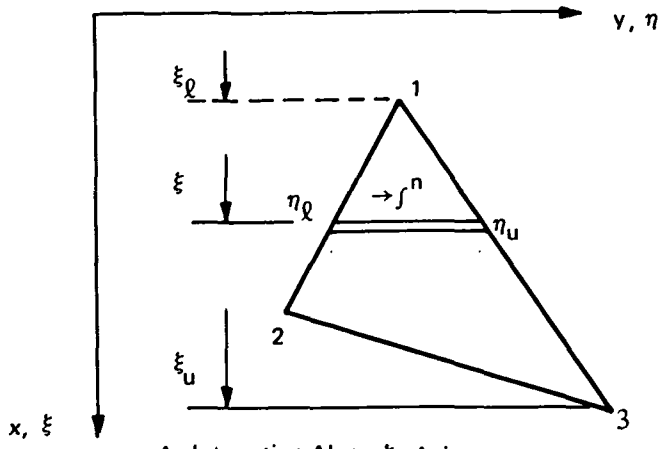

A. Integration Along ξ - Axis

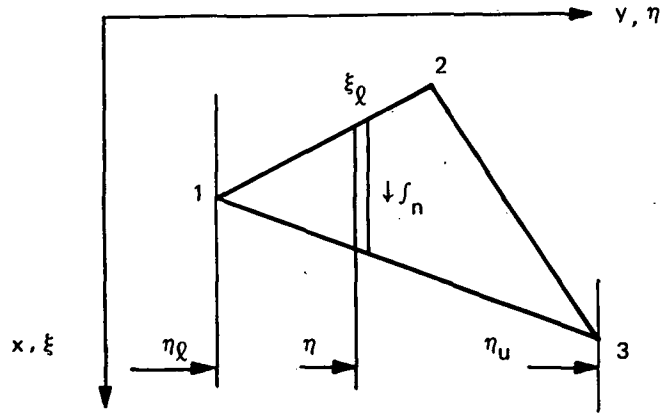

B. Integration along η - Axis

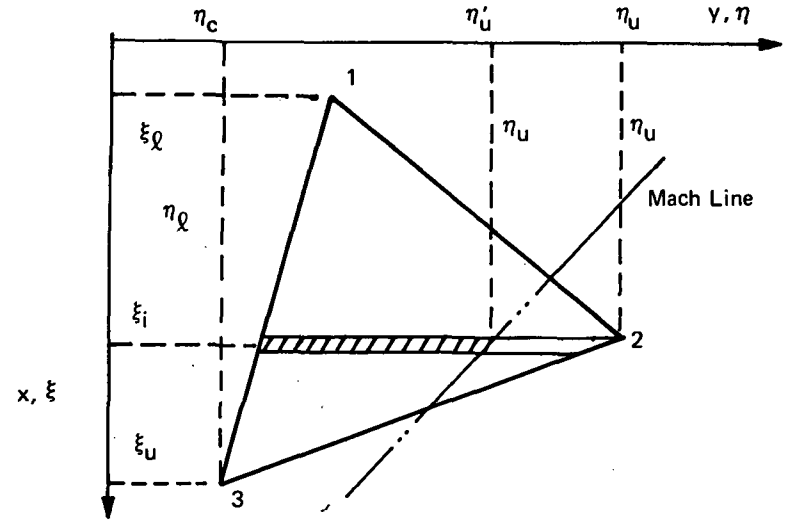

C. Partial Element Integration

Figure 14. Integration Scheme for Triangular Elements

Downwash Integrals

Assuming that the lifting surface is approximately parallel to the x-y plane, the normal velocity at the surface is given by

$$w\, e^{\lambda t} = \frac{1}{\ell}\frac{\partial \varphi}{\partial z}\, e^{\lambda t} \tag{A-13}$$

Using Watson's relation (Eqn. (A6)) in Eqn. (4), and performing the differentiation with respect to z, the nondimensional downwash matrix can be written as

$$W_{ij} = -\frac{1}{\pi\beta}\int_{\xi_\ell}^{\xi_u} e^{-i\hat{k}(x-\xi)}\left[\left\{\Omega(\xi,\eta_u)\frac{\partial\psi(\xi,\eta_u)}{\partial z} - \Omega(\xi,\eta_\ell)\frac{\partial\psi(\xi,\eta_\ell)}{\partial z}\right\} - \Omega_\eta\int_{\eta_\ell}^{\eta_u}\frac{\partial\psi(\xi,\eta)}{\partial z}\,d\eta\right]d\xi \tag{A-14}$$

The derivatives in (A14) can be changed to different bases more convenient for integration purposes. From (A7)

$$\frac{\partial\psi}{\partial z} = \frac{\partial\psi}{\partial\mu}\frac{\partial\mu}{\partial z} \tag{A15}$$

$$\frac{\partial\psi}{\partial\xi} = \frac{\partial\psi}{\partial\mu}\frac{\partial\mu}{\partial\xi} \tag{A16}$$

and therefore

$$\frac{\partial\psi}{\partial z} = \frac{\beta^2(z-\zeta)}{(x-\xi)}\frac{\partial\psi}{\partial\xi} \tag{A17}$$

Substituting Eqn. (A15-17) in Eqn. (A14), the downwash integral, after performing integration by parts and simplifying, becomes

$$W_{ij} = \frac{-\beta(z-\zeta)}{\pi}\left[I_1 - I_2\right] \tag{A18}$$

where $$I_1 = \int_{\xi_\ell}^{\xi_u}\frac{e^{-i\hat{k}(x-\xi)}}{(x-\xi)}\left\{\Omega_\xi\left(\psi(\xi,\eta_\ell) - \psi(\xi,\eta_u)\right)\right. \tag{A-19}$$

$$\left. + \frac{1+i\hat{k}(x-\xi)}{(x-\xi)}\left(\Omega(\xi,\eta_\ell)\,\psi(\xi,\eta_\ell) - \Omega(\xi,\eta_u)\,\psi(\xi,\eta_u)\right)\right\}d\xi$$

and $$I_2 = \Omega_\eta \int_{\eta_\ell}^{\eta_u} \left[\left\{ \frac{e - i\hat{k}(x - \xi_u)}{(x - \xi_u)} \psi(\xi_u, \eta) - \frac{e^{-i\hat{k}(x - \xi_\ell)}}{(x - \xi_\ell)} \psi(\xi_\ell, \eta) \right\} \right.$$

$$\left. - \int_{\xi_\ell}^{\xi_u} \psi(\xi, \eta) \frac{e^{-i\hat{k}(x - \xi)}}{(x - \xi)} \left(\frac{(1 + i\hat{k}(x - \xi))}{(x - \xi)} \right) d\xi \right] d\eta \qquad \text{(A-20)}$$

The first two terms in I_1 vanish when taken on the boundary of the triangle. The limits of integration in I_2 are as shown in Figure 14A, B, and C. Since the singularities have been eliminated in these integrals the limits of integration for the elements can extend up to the Mach cone. Numerical integration for Eqns (A11), (19) and (20) in the ξ and η senses proceed towards the element side furthest from the respective axis in all cases (See Figures 14A, B). Gaussian integration is performed for the now-analytical formulation of elements totally within and cut by the Mach cones. The limits of integration of the latter are determined by the conditions r or s = 0 as defined in Eq. (6). These limits are indicated on Figure 14C.

REFERENCES

1. Ashley, H.; Widnall, S.; and Landahl, M.T.: New Directions in Lifting Surface Theory. AIAA J., vol. 3, no. 1, Jan. 1965, pp. 3-16.

2. Landahl, M.T.; and Stark, V.J.E.: Numerical Lifting Surface Theory—Problems and Progress. AIAA J., vol. 6, no. 11, Nov. 1968, pp. 2049-2059.

3. Garrick, I.E.; and Rubinow, S.I.: Theoretical Study of Air Forces on an Oscillating or Steady Thin Wing in a Supersonic Main Stream. NACA Report 872, 1947.

4. Pines, S.; Dugundji, J.; and Neuringer, J.: Aerodynamic Flutter Derivatives for a Flexible Wing with Supersonic and Subsonic Edges. J. Aeron. Sci., vol. 22, no. 10, Oct. 1955, pp. 693-700.

5. Smith, G.C.C.: An Approximate Numerical Method of Calculating Three-Dimensional Supersonic Flutter Derivatives for Distortion Modes of Vibration. Bristol Aeroplane Co., Tech. Office, Rept. No. 80, Mar. 1954.

6. Zartarian, G.; Hsu, P.T.; and Voss, H.M.: Application of Numerical Integration Techniques to the Low-Aspect-Ratio Flutter Problem in Subsonic and Supersonic Flows. M.I.T. Aeroelastic and Structures Research Lab. Tech. Rept. 52-3, Oct. 1954.

7. Li, T.: Aerodynamic Influence Coefficients for an Oscillating Finite Thin Wing, Part I. Chance Vought Aircraft Inc. Rept. June 1954.

8. Zartarian, G.; and Hsu, P.T.: Theoretical Studies on the Prediction of Unsteady Supersonic Airloads on Elastic Wings, Parts I and II. WADC Tech Rept. 56-97, 1955.

9. Ashley, H.: Supersonic Air Loads on Interfering Lifting Surfaces by Aerodynamic Influence Coefficient Theory. The Boeing Co. Rept. No. D2-22067, Nov. 1962.

10. Moore, M.T.; and Andrew, L.V.: Unsteady Aerodynamics for Advanced Configurations, Parts I to IV. FDL-TDR-64-152, 1965.

11. Donato, V.W.; and Huhn, C.R.: Supersonic Unsteady Aerodynamics for Wings With Trailing Edge Control Surfaces and Folded Tips. AFFDL-TR-68-30, Aug. 1968.

12. Stark, V.J.E.: Calculation of Aerodynamic Forces on Two Oscillating Finite Wings at Low Supersonic Mach Numbers. SAAB TN53, Sweden 1964.

13. Appa, K.: Kinematically Consistent Unsteady Aerodynamic Coefficients in Supersonic Flow. Intl. J. for Numerical Methods in Eng'g., vol. 2, pp. 495-507, Oct. 1970. (Also National Aeronautical Laboratories NAL TN-9, India, Mar. 1968.)

14. Appa, K.; and Smith, G.C.C.: Further Developments in Consistent Unsteady Supersonic Aerodynamic Coefficients. AIAA, J. of Aircraft, vol. 9, no. 2, Feb. 1972.

15. Richardson, J.R.: A More Realistic Method For Routine Flutter Calculations. AIAA Symp., on Structural Dynamics and Aeroelasticity, Boston, Mass., Aug. 30 - Sept. 1, 1965.

16. Hassig, H.J.: An Approximate True Damping Solution of the Flutter Equation by Determinant Iteration. J. of Aircraft, vol. 8, no. 11, p. 885, Nov. 1971.

17. Argyris, J. H.: Continua and Discontinua. Proc. Air Force Conf. Matrix Methods Structural Mechanics. Wright-Patterson AF Base, Dayton, Ohio, 1965.

18. Evvard, J.C.: Use of Source Distributions for Evaluating Theoretical Aerodynamics of Thin Finite Wings at Supersonic Speeds. NACA TR 951, 1950.

19. Olsen, J.J.: Demonstration of a Supersonic Box Method for Unsteady Aerodynamics of Non-planar Wings, Parts I and II. FDL-TR-67-104, Feb. 1969.

20. Laschka, B.; et al: Generalized Aerodynamic Forces for Some Wing Planforms According to the Linearized Three-Dimensional Lifting Surface Theory in Subsonic and Supersonic Flow. VFW No. M-75/66, Dec. 1966. AGARD Structures and Materials Meeting. Ottawa, Sept. 1967.

21. Cunningham, H.J.: Application of a Supersonic Kernel-Function Procedure to Flutter Analysis of Thin Lifting Surfaces. NASA TN-D-6012, Nov. 1970.

22. Woodcock, D.L.; and York, E.J.: A Supersonic Box Collocation Method for The Calculation of Unsteady Air Forces of Tandem Surfaces. AGARD-CP-80-71 Part I, 1971.

23. Nelson, H.C.; Rainey, R.A.; and Watkins, C.E.: Lift and Moment Coefficients Expanded to the Seventh Power of Frequency for Oscillating Rectangular Wings in Supersonic Flow and Applied to a Specific Flutter Problem. NACA TN 3076, Apr. 1954.

24. Martin, J.C.; Diederich, M.S.; and Bobbitt, P.J.: A Theoretical Investigation of the Aerodynamics of Wing-Tail Combinations Performing Time-Dependent Motions at Supersonic Speeds. NACA TN 3072, May 1954.

25. Jones, W. P.: Supersonic Theory for Oscillating Wings of Any Planform. A.R.C R&M 2655, Great Britain, June 1948.

26. Allen, D. J.; and Sadler, D.S.: Oscillatory Aerodynamic Forces in Linearized Supersonic Flow for Arbitrary Frequencies, Planforms and Mach Numbers. ARC R&M 3415, Great Britain, 1963.

27. Heaslet, M.A.; Lomax, H.; and Jones, A.L.: Volterra's Solution of the Wave Equations as Applied to Three-Dimensional Supersonic Airfoil Problems. NACA Rept. No. 889, 1947.

28. Paine, A. A.: Development and Applications of Supersonic Unsteady Consistent Aerodynamics for Interfering Parallel Wings. User's Manual, Bell Aerospace Rept. No. 2471-956003. Programmer's Manual, Bell Aerospace Rept. No. 2471-956004. (Available as NASA-CR-112184 and NASA CR-112185)

29. Cunningham, H.J.: Total Lift and Pitching Moment on Thin Arrowhead Wings Oscillating in Supersonic Potential Flow. NACA TN 3433, May 1955.

NATIONAL AERONAUTICS AND SPACE ADMINISTRATION
WASHINGTON, D.C. 20546

OFFICIAL BUSINESS
PENALTY FOR PRIVATE USE $300

SPECIAL FOURTH-CLASS RATE
BOOK

POSTAGE AND FEES PAID
NATIONAL AERONAUTICS AND
SPACE ADMINISTRATION
451

U.S.MAIL

POSTMASTER: If Undeliverable (Section 158 Postal Manual) Do Not Return

"The aeronautical and space activities of the United States shall be conducted so as to contribute . . . to the expansion of human knowledge of phenomena in the atmosphere and space. The Administration shall provide for the widest practicable and appropriate dissemination of information concerning its activities and the results thereof."

—NATIONAL AERONAUTICS AND SPACE ACT OF 1958

NASA SCIENTIFIC AND TECHNICAL PUBLICATIONS

TECHNICAL REPORTS: Scientific and technical information considered important, complete, and a lasting contribution to existing knowledge.

TECHNICAL NOTES: Information less broad in scope but nevertheless of importance as a contribution to existing knowledge.

TECHNICAL MEMORANDUMS: Information receiving limited distribution because of preliminary data, security classification, or other reasons. Also includes conference proceedings with either limited or unlimited distribution.

CONTRACTOR REPORTS: Scientific and technical information generated under a NASA contract or grant and considered an important contribution to existing knowledge.

TECHNICAL TRANSLATIONS: Information published in a foreign language considered to merit NASA distribution in English.

SPECIAL PUBLICATIONS: Information derived from or of value to NASA activities. Publications include final reports of major projects, monographs, data compilations, handbooks, sourcebooks, and special bibliographies.

TECHNOLOGY UTILIZATION PUBLICATIONS: Information on technology used by NASA that may be of particular interest in commercial and other non-aerospace applications. Publications include Tech Briefs, Technology Utilization Reports and Technology Surveys.

Details on the availability of these publications may be obtained from:

SCIENTIFIC AND TECHNICAL INFORMATION OFFICE

NATIONAL AERONAUTICS AND SPACE ADMINISTRATION

Washington, D.C. 20546